

Quasars from the 7C Survey - I: sample selection and radio maps

Julia M. Riley¹, Steve Rawlings², Richard G. McMahon³,
Katherine M. Blundell², Philip Miller^{1,4}, Mark Lacy² & Elizabeth M. Waldram¹

¹*Mullard Radio Astronomy Observatory, Astrophysics Group, Cavendish Laboratory, Madingley Road, Cambridge, CB3 0HE.*

²*Astrophysics, Department of Physics, Keble Road, Oxford, OX1 3RH.*

³*Institute of Astronomy, Madingley Road, Cambridge, CB3 0HA.*

⁴*Present address: Venerable English College, Via di Monserrato, 45, 00186 Roma, Italy.*

13 October 2018

ABSTRACT

We describe the selection of candidate radio-loud quasars obtained by cross-matching radio source positions from the low-frequency (151 MHz) 7C survey with optical positions from five pairs of *EO* POSS-I plates scanned with the Cambridge Automatic Plate-measuring Machine (APM). The sky region studied is centred at RA 10^h 28^m, Dec +41° and covers ≈ 0.057 sr. We present VLA observations of the quasar candidates, and tabulate various properties derived from the radio maps. We discuss the selection criteria of the resulting ‘7CQ’ sample of radio-loud quasars. The 70 confirmed quasars, and some fraction of the 36 unconfirmed candidates, constitute a filtered sample with the following selection criteria: 151-MHz flux density $S_{151} > 100$ mJy; POSS-I *E*-plate magnitude $E \approx R < 20$; and POSS-I colour $(O - E) < 1.8$; the effective area of the survey drops significantly below $S_{151} \approx 200$ mJy. We argue that the colour criterion excludes few if any quasars, but note, on the basis of recent work by Willott et al. (1998b), that the *E* magnitude limit probably excludes more than 50 per cent of the radio-loud quasars.

Key words: radio continuum:galaxies – galaxies:active – quasars:general

1 INTRODUCTION

The advent of fast plate-measuring machines and extensive deep radio surveys with good positional accuracy has made possible the optical identification of large numbers of radio sources. Statistical studies can now be carried out using samples of radio sources associated with particular classes of optical object such as quasars. Surveys at low radio frequency allow the selection of samples of quasars which avoid the strong orientation biases inherent in samples selected at high radio frequencies: this is because the ratio of extended optically-thin radio emission to compact optically-thick radio emission increases rapidly with decreasing observing frequency, and it is the lat-

ter component which is greatly enhanced by Doppler boosting when radio-emitting material moves at a relativistic speed along a direction close to the line-of-sight. Thus, although low-frequency samples still contain some quasars whose total radio fluxes are strongly influenced by Doppler (i.e. orientation) effects, they are far out-numbered by objects for which the optically-thin (steep-spectrum) component dominates — we will refer to the latter as steep-spectrum radio-loud quasars (SSQs).

In Fig. 1 we show how recent work has extended the coverage of the low-frequency (151 MHz) radio lu-

minosity* L_{151} versus redshift z plane for SSQs. This provides a large range in L_{151} at a given z and *vice versa* — these are important requirements if the influences of L_{151} and z on the properties of SSQs are to be separately determined. However, no large samples selected at 151-MHz flux densities (S_{151}) below ~ 0.5 Jy have until now been constructed. As Fig. 1 shows, such samples would improve the L_{151} - z coverage still further. This provided the primary motivation for the project described in this paper.

The 7C surveys carried out with the Cambridge Low Frequency Synthesis Telescope (CLFST) at 151 MHz provide a perfect basis for this project because of their low limiting flux density, $S_{151} \sim 0.1$ Jy (e.g., McGilchrist et al. 1990; Lacy et al. 1995). Moreover, these surveys have a positional accuracy of a few arcsec and can be used to identify candidate quasars by comparison with optical plates. We chose to exploit these features by cross-matching the 7C positions with the positions of optical objects from the Palomar Observatory Sky Survey (POSS-I). We used the Automatic Plate-measuring Machine (APM) at Cambridge to scan the glass copies of the original Palomar Observatory Sky Survey (POSS-I) covering a continuous area of the 7C survey; in the search for quasar candidates we sought identifications (IDs) on both the *E* and *O* POSS-I plates to minimise any selection biases due to object colour.

The organisation of this paper is as follows. In Sec. 2 we describe the selection of the candidate radio-loud quasars. In Sec. 3 we describe the VLA observations of 134 of these candidates and in Sec. 4 we present the results of these observations. In Sec. 5 we discuss the causes of incompleteness in the resulting sample of radio quasars which we will henceforth refer to as the 7CQ sample. In a companion paper (Rawlings et al., in prep.; hereafter Paper II) the optical spectra of the quasar candidates will be presented, and further properties of the sample discussed.

B1950.0 co-ordinates are used, and the convention for radio spectral index (α) is that $S_\nu \propto \nu^{-\alpha}$, where S_ν is the flux density at frequency ν .

2 SAMPLE DEFINITION

We chose one area of the CLFST 7C survey centred at RA $10^{\text{h}} 28^{\text{m}}$ and Dec $+41^\circ$ (McGilchrist et al. 1990) for our new study of SSQs; a typical value for the limiting (5σ) flux density over this area is 80 mJy (for point sources) but in some parts it is as high as ≈ 200 mJy, and the 1σ positional errors range from ~ 2 arcsec for sources with flux densities > 1 Jy to ~ 10 arcsec for the faintest sources.

Five pairs of POSS-I plates were scanned (*EO690*, *EO709*, *EO711*, *EO1032* and *EO1348*). A

catalogue was constructed of all the optical objects with stellar images on both the *E* and *O* plates which were within 15 arcsec of a radio source; there were 175 such objects, of which 7 were on two adjacent POSS-I plates. A statistical analysis described in Sec. 5 indicated that a significant fraction of these objects are random coincidences, particularly those for which the radio-optical separation is greater than 10 arcsec.

We decided therefore to concentrate follow-up work on those objects with radio-optical separations (r) of less than 10 arcsec. Further higher resolution radio observations were required to eliminate the remaining chance associations. We therefore made VLA observations of those sources in the sample with $S_{151} > 0.1$ Jy, and $r < 10$ arcsec; due to pressure on observing time a small fraction (~ 10 per cent) of the sources were omitted. Some sources were omitted either because they were very extended at 151 MHz (> 40 arcsec), or because they had already been observed with the VLA. Other sources were omitted randomly if there were too many targets in a particular RA range during the VLA observations. Another source of essentially random exclusion arose because of minor changes in sample membership to be discussed in the following paragraph. We also chose to eliminate some sources from our VLA mapping programme because of their red (optical) colours; the reasons for this are discussed in Sec. 5 (these sources were mainly associated with the *EO709* POSS-I plate pair). Some of the sources with r in the range 10–15 arcsec were also observed with the VLA if the optical object seemed likely, on the grounds of colour, to be a quasar.

Subsequently the optical plates were re-scanned and the APM data re-calibrated. This allowed for a number of minor improvements to the APM analysis procedures (which were then identical to those described by Lacy et al. 1995). A new catalogue was constructed of all the optical objects which were stellar on either the *E* or the *O* plates, or on both, with $r < 10$ arcsec; it contains 206 entries of which six were repeated measurements of an optical object on two pairs of plates, and four were radio sources each matched with two possible optically-unresolved IDs (we excluded the two radio sources found serendipitously in one field, category ‘T’ in Table 1, since they fail the $r < 10$ arcsec criterion). There are thus 196 possible 7C/APM cross matches in this revised main sample. There are fairly minor differences between this and the initial catalogue which relate to re-classification of some of the optical objects. Table 1 contains the main sample and was constructed from the second catalogue since this is more reliable (sources not in the first catalogue are flagged). Table 2 lists a subsidiary sample consisting of 26 additional cross-matches which were from the first version of the catalogue either with $10 < r < 15$ arcsec (and with the blue colours expected for quasars) or with

* We take $H_0 = 50 \text{ km s}^{-1} \text{ Mpc}^{-1}$, $q_0 = 0.5$ and a cosmological constant of zero.

Figure 1. The coverage of the L_{151} versus z plane for various samples of SSQs. The location of SSQs within the 3C and 7C complete redshift surveys are shown by the shaded regions; the lower bounds of these regions correspond to $S_{178} = 10.9$ Jy and $S_{151} = 0.5$ Jy in each case taking $\alpha = 0.8$. SSQs from the Molonglo/APM Quasar Survey (MAQS), and also from the similarly-selected Molonglo Quasar Survey (MQS), lie above the solid line (which corresponds to a 408-MHz flux density limit of 0.95 Jy taking $\alpha = 0.8$). SSQs from the B3-VLA survey are shown by asterisks. Note that the B3-VLA, MAQS and MQS surveys are all based on radio catalogues selected at 408 MHz. Details of all these samples can be found in the following references: the revised 3C sample – Laing, Riley & Longair (1983); the 7C Redshift Survey – Willott et al. (1998b), and in prep.; the MAQS – Serjeant et al. (1998), and in prep.; the MQS (Kapahi et al. 1998); the B3-VLA survey – Vigotti et al. (1997). SSQs from the 7CQ sample (described in this paper) lie above the dashed line which corresponds to $S_{151} = 0.1$ Jy taking $\alpha = 0.8$.

$r < 10$ arcsec but not in the second catalogue (due to optical re-classification).

The total sky coverage of the 7CQ sample is the area of the five POSS-I plate pairs, or about 0.057 sr. The limiting optical magnitudes of the POSS-I plates are $O \sim B \approx 21.5$ and $E \approx R \approx 20$, and the typical uncertainty in an $O - E$ colour is about 0.5 magni-

tudes. The reliability of the APM classification algorithm, i.e. establishing whether objects are unresolved or extended, varies with object magnitude. Only for objects about two magnitudes brighter than the plate limit is it possible to separate point-like optical objects from extended objects with very high reliability. Close to the plate limit circular and/or small galaxies

are indistinguishable from point-like quasars. One of the objects, while selected in the initial version of the catalogue, was not selected in the final version (and hence is listed only in Table 2) because of optical reclassification: it is now classified by the APM analysis as extended, but is a spectroscopically-confirmed high-redshift quasar (Paper II). There is thus a small risk of falsely excluding point-like optical objects at the fainter optical magnitudes. These issues will be discussed further in Section 5.2.

The 151 MHz flux density completeness limit varies across each 7C field because of the primary beam polar diagram, geometric and other distortions of the beamshape (McGilchrist et al. 1990), and because of fluctuations in the local noise level. We have calculated the fraction A_{frac} of the total 7CQ survey area of 0.057 sr which is complete to a given limiting flux density S_{lim} taking all these effects into account, and this is plotted in Fig. 2. At $S_{\text{lim}} > 0.1$ Jy a suitable functional approximation to this curve is given by $A_{\text{frac}} = (1 + e^{-a(S_{\text{lim}}-b)})^{-1}$ with $a = 39.72$ and $b = 0.0573$. This approximate functional form will be used in Paper II.

Figure 2. The fraction A_{frac} of the 7CQ area which is complete to a given 151 MHz limiting flux density S_{lim} . The dashed line shows the fit to the data at $S_{\text{lim}} > 0.1$ Jy discussed in Sec. 2.

(1)	(2)	(3)	(4)	(5)	(6)	(7)	(8)	(9)	(10)	(11)	(12)	(13)	(14)	(15)
	RA(B1950)	Dec(B1950)	r	O	$O - E$	ΔRA	ΔDec	S_{151}	S_{1490}	α_{151}^{1490}	S_{core}	θ	Opt	
	09 55 32.61	43 30 40.9	2.1	20.64	1.39	-0.07	1.5	690	174	0.60	174.0	≤ 0.3	QC	N
	09 55 49.88	42 51 25.9	4.2	18.13	.53	-0.06	0.5	520	87	0.78	20.4	11.0	QC	Y
	09 56 34.8	40 29 52.0	6.4	17.83	1.44	0.42	6.6	1080	(118)	(0.99)		8.0	S	V
	09 58 07.4	42 44 07	9.4	21.63	2.49	0.09	-9.8	180	(m)			7C(43)	?	N ^r
	09 58 31.39	41 21 19.0	6.8	19.97	1.31	-0.04	0.5	420	54	0.90	1.5	12.0	QC	Y
	09 58 37.59	42 23 38.9	6.8	19.51	2.60	0.16	-2.2	230	45	0.71	45.0	0.9	S	Y
	09 59 14.5	40 48 50	3.2	21.04	2.37	0.62	-5.5	280	24	1.07		34.0	M	Y
	09 59 27.06	40 07 39.6	7.7	18.89	2.27	-0.48	-11.9	280	33	0.93	33.0	1.1	M	Y
N	10 00 46.07	41 33 57.6	7.5	21.70	2.25	0.90	-13.5	200	(29.8)	(0.85)		39.0	M	F
	10 01 20.79	42 33 52.8	5.5	16.97	1.49	0.25	7.2	890	76	1.07		2.4	M	Y
	10 01 36.45	45 07 27.5	9.8	15.81	.98	-0.16	-11.8	130	14.4	0.96	14.4	≤ 0.3	M	N
	10 01 39.73	40 51 21.6	6.2	20.95	1.70	-0.03	0.0	130	52	0.40	39.0	17.0	Q	Y
	10 01 53.98	50 34 05.3	2.9	20.14	1.44	-0.03	0.7	150	(73.8)	(0.32)		(19.0)	OC0(c)	C
	10 02 05.90	48 20 08.7	2.8	17.57	.50	-0.04	-0.4	640	186	0.54	186.0	0.4	Q	N
N	10 03 28.8	43 13 20.3	3.4	20.86	2.76	0.20	2.8	360	(76.2)	(0.70)		(70.0)	EC1	C

Table 1. A summary of the radio and optical properties of the candidate 7CQ quasars in the main sample. **Column 1** contains flags with meanings as follows: N indicates that the source was not in the first version of the optical catalogue; R indicates a repeat entry because the optical object occurs in 2 POSS-I fields; S indicates that there is more than one optically-unresolved object in the field of the source; * indicates that this proposed identification failed the original selection criterion on r (see column 4); and T indicates that there is more than one radio source in the field. The RAs and Decs of the radio sources are given in **Columns 2 & 3**: the positions were measured from the radio core if present (i.e., if there is an entry in column 12); where there is no core the position is midway between the radio hotspots, or the centroid of the radio emission; if the source has not been observed at high resolution with the VLA, the position is taken from the NVSS catalogue (Condon et al. 1998) or (in a few cases marked 7C in column 13) the 7C catalogue (McGilchrist et al. 1990). **Column 4**: values of r , the separation (in arcsec) of the 7C radio source position and the APM optical position. **Columns 5 and 6**: the magnitude of the quasar candidate on the POSS-I O-plate, and its colour (the difference between its magnitudes on the O- and E-plates). **Columns 7 and 8**: the differences in RA (in seconds of time) and Dec (in arcsec) between the radio position given in columns 2 and 3 and that of the quasar candidate (in the sense radio minus optical). **Column 9**: the flux density in mJy at 151 MHz S_{151} from the 7C catalogue. **Column 10**: the flux density in mJy either at 1.49 GHz from our own VLA observations or (in parentheses) at 1.40 GHz from the NVSS survey. In a few cases, marked (m), there is no corresponding source in the NVSS survey and/or no source was detected in higher resolution VLA observations to a typical surface brightness upper limit of ~ 1 mJy per beam on low-resolution (4 arcsec FWHM) maps made either from our own observations or from the FIRST Survey data of Becker, White & Helfand (1995). **Column 11**: the spectral index, α , between 151 MHz and 1.49 (or 1.4) GHz; (c) indicates that no value has been calculated because the value of S_{151} is severely over-estimated because of source confusion. **Column 12**: the flux density of the core in mJy at 1.49 GHz. For well-resolved sources this is the height of the peak (in mJy per beam) at the core position. For less well-resolved sources in which it is impossible to distinguish the core from the surroundings it is the total flux density given in column 10. **Column 13**: the angular size of the source in arcsec. A question mark flags an uncertainty which is discussed in the notes on that source. If the entries in columns 10 and 12 are the same the size was measured by fitting a Gaussian with the AIPS task IMFIT. Otherwise the size was measured from the map. A value in parentheses is the largest angular size given in the NVSS catalogue (or the 7C catalogue, if preceded by 7C, with a 'c' denoting that the 7C catalogue entry is a confusion of two or more sources). **Column 14**: optical type, classified as follows: Q - spectroscopically-confirmed quasar (see paper II); QC - good ID which is optically unresolved but which has not yet been spectroscopically confirmed as a quasar or galaxy; S - proposed ID is a star; M - proposed ID rejected on positional grounds; G - confirmed galaxy; BL - confirmed BL Lac object; ? - stellar on both the O and E plates but ID not yet certain due to lack of follow-up with the VLA and optical spectroscopy; EC1, EC2 - the object is non-stellar (1) or confused (2) on the E-plate; OC0, OC1, OC2 - the object is noise-like (0), non-stellar (1) or confused (2) on the O-plate. Note that some of the spectroscopically-confirmed quasars are not classified by the APM analysis as stellar on both POSS-I plates. A (c) in this column indicates that the optical object is very likely to be an ID - the criterion being that the NVSS and APM positions differ by < 2 arcsec for unresolved radio sources, and < 6 arcsec for resolved sources. **Column 15** contains flags associated with the radio data: a Y indicates that a map is presented in Fig. 3 with a lower case y indicating that additional notes are to be found in the text; N indicates that a map was made but is not shown in Fig. 3 (typically because the source is unresolved) with lower case n, again, advertising additional notes in the text; C indicates that the only map available is from the NVSS low-resolution VLA survey of Condon et al. (1998); ‡ means excluded from our high-resolution VLA follow-up because $S_{151} \leq 100$ mJy, r means excluded because of the red optical colour of the proposed ID (see Section 5), l means excluded because of large 7C angular size, and j means excluded randomly. Other letters refer to additional sources of high-resolution radio maps: D, Law-Green et al. (1995); F, FIRST survey archive (Becker et al. 1995); M, Machalski & Condon (1986); L, Riley & Warner (1994); P, Patnaik et al. (1992); V, Vigotti et al. 1989. One entry in the 7C catalogue (at position 10 24 04.2, +48 43 30) is an alias of a bright radio source, and its candidate identification a star.

(1)	(2)	(3)	(4)	(5)	(6)	(7)	(8)	(9)	(10)	(11)	(12)	(13)	(14)	(15)
	RA(1950)	Dec(1950)	r	O	$O - E$	Δ RA	Δ Dec	S_{151}	S_{1490}	α_{151}^{1490}	S_{core}	θ	Opt	
	10 03 55.4	38 27 56	8.1	19.57	.78	-0.66	-2.2	160	(m)			7C(71)	S	N
	10 05 31.10	45 33 23.3	6.4	19.66	.87	-0.57	-1.7	120	23	0.72		3.3	M	Y
N	10 05 53.5	41 00 58	7.9	21.58	1.87	0.43	5.6	160	(m)				EC1	F
	10 06 33.2	47 10 08	5.3	20.69	.80	0.14	-2.8	450	77	0.77		7.0	Q/EC1	Y
	10 06 47.28	45 12 41.5	4.5	20.36	1.43	-0.46	10.4	80	(14.0)	(0.78)		(23.9)	?	C‡
	10 07 44.81	36 36 36.6	4.5	21.38	1.77	-0.10	3.7	160	23	0.85	23.0	≤ 0.3	QC	N
N	10 07 52.96	34 24 41.7	1.3	15.29	.99	0.44	11.0	90	(15.3)	(0.80)		23.0	M	F‡
	10 07 57.46	33 45 05.2	4.5	19.98	.04	-0.13	-0.2	230	376	-0.21	376.0	≤ 0.3	Q	N
	10 07 59.11	38 32 23.0	4.1	19.91	.60	0.02	0.3	290	49	0.78	15.0	42.0	Q	Y
	10 09 17.53	33 24 16.2	4.2	17.99	.40	-0.15	-1.2	570	(195)	(0.48)		(< 17)	Q	C
	10 09 21.46	40 44 24.2	3.3	21.75	2.42	-0.01	-0.8	130	13	1.0		3.5	QC	y
	10 09 23.3	36 54 18	4.9	16.53	1.20	-0.17	-5.1	370	47	0.90		60.0	M	Y
	10 09 24.0	42 03 18	4.4	18.87	2.39	-0.12	-4.0	390	(m)			7C(65)	S	N
N	10 09 42.36	42 44 48.2	1.1	18.13	1.56	-0.08	0.8	180	(79.5)	(0.36)		(< 19)	EC1(c)	C
	10 09 48.44	36 08 39.2	6.3	18.62	.89	-0.04	0.1	180	25	0.85	25.0	0.6?	Q	y
	10 09 54.24	38 34 33.4	6.0	21.24	3.43	-0.14	-1.4	360	54	0.83	2.4	32.0	S	Y
N	10 09 58.96	46 10 31.7	5.4	21.74	3.53	0.10	2.7	160	(46.1)	(0.56)		(< 16)	EC2	C
	10 10 20.74	49 33 33.5	3.6	19.35	.66	-0.09	0.6	210	285	-0.13	285.0	≤ 0.3	Q	N
	10 10 32.9	47 48 49	8.6	19.50	1.59	0.81	0.0	110	(m)			7C	?	-j
	10 10 46.37	42 04 02.6	1.5	19.60	.94	0.02	1.1	500	72	0.85	2.1	21.0	QC	Y
N	10 11 13.89	40 08 07.5	7.7	19.58	.48	0.06	-0.3	100	(45.5)	(0.35)	43.9	14.0	EC1(c)	F‡
	10 11 17.65	41 27 12.0	7.1	20.56	1.09	0.05	1.3	130	46	0.47	37.0	3.0	QC	Y
	10 11 27.34	40 58 21.2	8.2	17.41	1.12	-1.74	2.5	310	(30.8)	(1.04)		33.0	M	F
	10 11 44.58	44 36 28.4	1.2	18.96	.39	-0.04	0.0	450	69	0.82	4.0	34.0	Q	Y
	10 11 55.26	49 40 56.4	1.9	16.47	.96	-0.09	0.4	690	370	0.27	344.0	2.0	BL	Y
	10 12 32.25	39 22 22.8	7.3	20.43	1.46	0.14	-0.6	110	15	0.88	10.0	1.2	Q/EC1	N
	10 12 47.1	32 42 02	7.9	20.71	1.77	0.58	-4.1	910	(110)	(0.95)		43.0	M	Y
	10 12 50.2	40 20 18	6.7	21.06	3.25	-0.48	-12.0	300	31	0.99		65.0	M	Y
N	10 12 52.69	39 35 16.3	8.0	21.44	2.67	0.55	-10.9	380	(56.3)	(0.86)		29.0	M	F
	10 13 21.83	36 24 35.7	4.7	18.42	2.74	0.34	2.4	640	61	1.03	47.0	2.0	M	Y
N	10 13 24.60	46 58 41.1	8.4	19.75	2.56	-0.54	4.5	530	(137)	(0.61)		(27.0)	?	C ^j
	10 14 18.96	46 34 11.5	7.0	20.41	.70	0.62	-5.8	150	33	0.66	33.0	≤ 0.3	M	N
	10 14 26.91	38 47 54.5	5.6	16.15	.94	0.43	14.4	80	(20.8)	(0.60)		< 5	S	F‡
	10 14 46.25	46 25 15.7	4.8	19.43	.51	-0.07	-0.6	230	42	0.74	3.8	14.0	Q	Y
N	10 14 55.67	45 48 02.4	9.9	19.63	2.00	1.30	6.4	120	(18.2)	(0.85)		(19.7)	?	C ^j
	10 14 56.71	44 14 50.7	5.6	18.97	.72	0.02	1.2	110	24	0.67		3.0	Q	Y
	10 15 04.90	46 20 24.8	2.9	20.48	1.07	0.19	-2.9	550	61	0.96		6.0	Q/OC1	Y
	10 15 16.23	35 57 41.3	3.6	18.64	.93	-0.07	0.2	490	580	-0.07	560.0	4.8	Q	Y
	10 15 36.56	43 37 34.6	1.4	20.69	.78	-0.08	0.8	340	45	0.88	25.0	4.0	Q	Y
N	10 16 35.86	33 53 14.3	9.8	21.42	1.68	0.16	-8.6	100	(7.7)	(1.15)		(< 34)	?	C‡
	10 16 41.74	42 59 01.4	3.1	19.76	1.18	0.24	14.7	160	(25.8)	(0.82)		(30.5)	S	C
	10 16 42.40	34 28 02.2	7.2	17.68	1.16	0.13	23.1	70	(7.7)	(0.99)		(< 34)	S	C‡
	10 16 49.79	38 48 35.7	5.6	18.56	2.38	-0.12	-2.0	1020	(54.6)	(1.31)		76.0	S	F
N	10 17 19.48	46 11 41.7	0.5	21.34	3.36	-0.06	-1.2	120	(36.8)	(0.53)		(18.2)	EC1(c)	C
N	10 17 48.31	48 46 24.3	5.7	20.17	1.54	-0.33	48.1	9300	(10.3)	(c)		(< 23)	M	C
	10 18 03.44	45 38 39.0	2.6	18.16	.50	-0.02	-0.6	630	(131.1)	(0.70)	47.0	45.0	Q	Y
N	10 18 08.75	50 05 47.4	5.9	21.25	2.87	-0.05	-0.6	310	(52.9)	(0.79)		29.2	EC1(c)	C
	10 18 11.08	44 50 08.4	1.8	20.73	1.19	-0.01	-0.3	240	54	0.65	54.0	≤ 0.3	Q	N
	10 18 24.11	34 52 29.2	2.3	17.77	.56	-0.07	-0.5	1020	(457.4)	(0.36)	371.0	19.0	Q	M
	10 18 41.01	40 46 55.9	2.5	19.27	.99	0.00	1.2	860	128	0.83	3.7	11.0	QC	Y
	10 18 47.80	32 42 46.2	1.7	20.13	1.16	0.04	-0.4	2500	247	1.01	54.0	9.0	Q	Y
N	10 19 05.59	46 11 20.1	1.6	21.51	2.00	-0.23	-0.8	860	(129.6)	(0.85)		(20.9)	EC1(c)	C
	10 19 12.25	37 13 47	6.2	20.82	1.06	0.10	4.6	1320	233	0.76		30.0	M	Y
	10 19 31.30	37 50 45.0	8.8	20.90	1.34	-0.01	2.5	250	14	1.27	10.1	2.0	QC	y
	10 19 33.07	45 56 15.4	8.0	20.71	1.18	0.04	-0.6	650	134	0.69	23.0	42.0	Q	Y
	10 19 40.56	39 47 00.3	9.3	17.04	.79	0.10	-0.4	310	115	0.43	42.0	25.0	Q	Y
	10 19 56.13	34 06 08.5	1.6	19.53	1.00	-0.05	-0.3	670	80	0.93	2.3	37.0	Q	Y
N	10 20 03.24	43 40 24.0	3.8	21.68	3.78	0.05	3.3	430	(109.4)	(0.61)		(< 17)	EC1	C

Table 1. (cont).

(1)	(2)	(3)	(4)	(5)	(6)	(7)	(8)	(9)	(10)	(11)	(12)	(13)	(14)	(15)
	RA(1950)	Dec(1950)	r	O	$O - E$	ΔRA	ΔDec	S_{151}	S_{1490}	α_{151}^{1490}	S_{core}	θ	Opt	
	10 20 05.94	48 06 57.5	1.6	19.70	.82	-0.04	1.1	2570	470	0.74	470.0	0.6	Q/EC1	Y
	10 20 14.6	40 03 28.0	4.0	17.38	.70	0.11	1.7	2960	(1123)	(0.44)		< 5	Q	V
R	10 20 14.6	40 03 28.0	4.0	17.25	.54	-0.07	1.8	2960	(1123)	(0.44)		< 5	Q	V
	10 20 17.31	43 47 15.8	9.0	12.37	.98	1.19	4.2	280	(33.0)	(0.96)		(< 19)	S	C
	10 20 21.70	36 19 46.9	2.5	20.18	1.01	-0.05	0.3	140	(29.2)	(0.70)	19.1	16.0	Q	F
	10 20 24.68	48 39 48.7	0.4	20.32	.53	0.02	-0.1	2200	(240)	(0.99)	5.0	43.0	Q	Y
	10 21 14.24	39 53 13.9	8.0	20.13	1.14	-0.10	17.9	130	17	0.89		2.0	M	Y
R	10 21 14.24	39 53 13.9	9.4	20.30	1.21	-0.29	18.0	130	17	0.89		2.0	M	Y
N	10 21 57.99	37 08 33.0	1.0	20.84	1.30	0.50	11.4	90	(19.3)	(0.69)		(27.9)	?	C‡
	10 22 07.62	39 19 04.8	5.2	21.39	1.41	-0.03	-0.3	120	24	0.70	24.4	1.2	Q	Y
	10 22 46.73	43 32 51.5	6.9	18.40	1.09	-0.07	1.2	430	(57.5)	(0.90)	5.0	35.0	QC	y
N	10 22 52.10	35 06 06.2	5.0	20.37	2.69	-0.10	-0.4	550	(110)	(0.72)		(28.9)	EC1(c)	F
	10 23 08.98	35 53 52.3	2.2	19.44	1.24	0.41	-20.8	130	(20.2)	(0.84)	8.5	0.7	M	N
	10 23 51.31	37 13 43.1	1.4	20.98	1.77	-0.05	0.0	180	173	0.02	173.0	≤ 0.3	Q	N
	10 24 01.64	41 54 42.9	7.6	18.63	.45	-0.04	0.1	490	(90.1)	(0.76)	1.1	50.0	Q	y
	10 24 06.92	46 46 14.3	9.1	19.81	.42	0.04	-0.5	130	16	0.92	14.4	2.2	QC	Y
	10 24 09.47	48 18 31.7	0.6	19.46	.67	0.02	0.3	770	233	0.52	164.0	6.0	Q	Y
N	10 24 14.39	39 23 24.6	1.8	21.22	4.84	-0.16	1.9	420	(43.9)	(1.01)		(< 19)	EC2	C
	10 24 26.59	43 07 19.7	5.3	19.23	.68	-0.07	0.8	300	59	0.71		10.0	QC	Y
N	10 24 29.6	48 32 46	8.9	20.98	3.24	-0.22	8.5	6600	(987)	(0.85)		(69.0)	EC1	C
	10 24 54.03	36 12 51.7	2.5	18.97	.83	-0.01	-0.3	200	(47.1)	(0.65)	5.2	61.0	QC	Y
	10 25 34.59	43 21 47.5	3.3	19.20	.82	-0.08	1.0	550	94	0.77	10.3	39.0	Q	Y
N	10 26 36.88	37 49 08.8	9.4	18.84	2.22	-0.73	13.9	250	(66.1)	(0.60)		≤ 4	M	F
	10 27 08.83	32 39 42.8	9.7	19.71	.57	0.00	-0.6	210	100	0.32	98.0	4.0	Q	Y
	10 27 23.44	43 24 31.7	2.8	19.72	.72	-0.03	0.5	700	115	0.79	36.0	8.0	Q	Y
	10 27 24.64	34 01 56.0	4.2	20.41	.59	0.02	-0.9	160	14	1.06		2.0	Q/EC1	Y
	10 28 10.62	41 34 00.9	9.7	20.97	2.90	0.64	6.3	130	25	0.71	25.2	0.4	M	y
	10 28 47.81	42 09 46.9	3.1	18.21	.69	-0.03	0.3	1610	215	0.88	2.1	41.0	Q	Y
N	10 28 59.3	35 17 44	9.2	21.38	1.83	-0.66	4.6	3000	(c)			7C(c)	M	D
	10 29 31.32	49 48 11.0	0.9	21.06	1.28	0.07	1.0	200	46	0.64	9.0	16.0	Q	y
	10 29 47.42	37 53 54.4	1.7	18.04	.86	0.05	0.8	320	72	0.65	37.0	6.0	QC	Y
	10 29 52.44	39 25 37.8	7.0	18.77	.66	-0.06	-0.3	120	(25.2)	(0.70)	6.4	6.6	Q	Y
	10 30 07.80	41 31 34.5	4.0	18.36	1.00	-0.05	0.4	980	547	0.25	481.0	5.0	Q	Y
	10 31 09.6	49 46 40	8.2	21.02	1.25	-0.43	-0.9	160	31	0.72		8.0	M	Y
	10 32 21.14	45 26 17.9	5.5	19.22	1.85	0.15	10.4	160	26	0.79		7.3	M	Y
	10 32 21.21	34 21 56.9	2.1	18.34	.41	0.06	-1.3	510	117	0.64	44.0	44.0	QC	Y
	10 32 34.50	44 25 03.7	5.8	20.37	1.66	-0.07	0.7	120	36	0.52	24.9	5.0	QC	Y
	10 32 58.36	38 12 14.5	7.9	17.14	.26	0.10	1.3	140	54	0.42	45.0	2.0	Q	Y
	10 33 13.62	48 22 44.4	8.0	21.21	1.25	-0.07	8.4	440	73	0.78	73.0	1.3	M	Y
N	10 33 25.15	36 49 54.3	8.2	20.88	2.31	0.05	0.3	90	(75.5)	(0.08)		(< 18)	EC1(c)	C‡
	10 33 50.91	33 36 41.3	7.4	19.15	1.08	0.16	9.5	100	(23.2)	(0.66)		(< 20)	OC1	C‡
N	10 33 59.50	34 27 00.2	8.8	21.55	1.72	-0.87	15.6	130	(18.6)	(0.87)		(27.4)	M	F
N	10 34 00.75	38 47 13.2	9.6	20.67	2.93	0.11	5.1	130	(19.6)	(0.85)		(28.8)	OC1	F
	10 34 08.5	46 09 23	7.8	20.70	2.83	-0.63	45.8	230	18	0.84		6.0	M	y
T	10 34 10.1	46 07 46	7.8						3			2.0	M	y
T	10 34 17.2	46 09 58	7.8						12			5.0	M	y
	10 34 15.93	47 05 49.4	0.5	19.88	.56	0.01	-0.1	500	89	0.75	52.0	4.0	Q/OC1	Y
R	10 34 15.93	47 05 49.4	0.5	19.17	.52	0.00	0.2	500	89	0.75	52.0	4.0	Q/OC1	Y
N	10 34 22.63	43 50 51.0	8.7	11.86	3.28	-0.25	0.9	210	(132.5)	(0.21)		(< 19)	G	C
N	10 34 22.42	45 40 14.3	9.9	21.39	1.53	-1.11	-12.5	90	(11.8)	(0.91)		(< 31)	EC1	C‡
R	10 34 22.42	45 40 14.3	9.5	20.55	1.03	-1.32	-10.8	90	(11.8)	(0.91)		(< 31)	?	C‡
N	10 34 39.52	39 43 28.5	8.8	19.40	2.64	-1.45	-0.1	230	(28.7)	(0.93)		42	M	F
N	10 34 50.86	45 44 07.2	5.4	21.76	1.81	0.28	-4.1	90	(21.3)	(0.65)		(19.7)	OC1(c)	C‡
	10 35 06.94	38 56 12.9	2.8	17.50	.64	-0.22	17.6	170	18	0.98		2.3	M	Y
	10 35 17.4	48 41 24	2.2	19.77	.84	-0.05	0.8	2080	226	0.97		22.0	Q	Y
	10 35 36.99	50 03 13.7	1.5	20.93	1.03	0.04	0.5	1070	124	0.94	4.9	24.0	Q	Y
R	10 35 36.99	50 03 13.7	2.6	20.93	1.80	-0.13	2.3	1070	124	0.94	4.9	24.0	Q	Y
N	10 35 47.50	46 33 17.9	4.9	21.09	1.35	-0.11	1.8	150	(36.2)	(0.64)		(16.6)	EC1(c)	C

Table 1. (cont).

(1)	(2)	(3)	(4)	(5)	(6)	(7)	(8)	(9)	(10)	(11)	(12)	(13)	(14)	(15)
	RA(1950)	Dec(1950)	r	O	$O - E$	ΔRA	ΔDec	S_{151}	S_{1490}	α_{151}^{1490}	S_{core}	θ	Opt	
	10 36 00.86	49 47 16.1	0.4	21.11	2.24	0.01	1.7	210	(34.7)	(0.81)		(37.5)	?(c)	C ^r
	10 36 16.57	47 21 18.9	1.2	20.98	2.08	-0.04	-0.1	3800	(381.6)	(1.03)		(< 19)	?(c)	C ^r
	10 36 23.04	41 19 42.9	4.8	21.24	2.96	0.06	-1.3	160	22	0.86	22.4	0.7	QC	N
	10 36 36.52	50 07 18.3	7.6	19.83	1.16	0.61	-1.4	290	(33.5)	(0.97)		(< 20)	QC	C
N	10 36 44.43	48 18 22.9	7.3	20.87	3.29	-0.93	7.6	240	(22.6)	(1.06)		(< 26)	?	C ^r
	10 37 01.66	42 41 17.4	0.5	20.38	1.33	-0.11	0.9	700	107	0.82	2.2	25.0	Q/EC1	Y
	10 37 25.93	45 05 16.7	6.5	19.11	.52	-0.09	-0.5	110	(23.7)	(0.69)	10.0	1.0	Q/OC1	Y
	10 37 44.72	45 45 13.2	7.8	18.51	.70	-0.06	0.4	140	(60.0)	(0.38)		(< 19)	Q	C ^j
	10 38 09.41	43 13 05.1	1.2	19.12	.79	-0.01	0.6	790	100	0.90	8.0	10.0	Q	Y
N	10 38 47.48	40 05 01.0	4.9	21.24	3.27	0.06	-0.5	100	(35.8)	(0.46)	3.8	38.0	EC1(c)	F‡
	10 38 51.52	46 49 16.9	5.5	19.37	.40	-0.03	-1.1	120	29	0.63	28.6	1.1	Q	Y
N	10 39 01.49	46 31 56.1	4.4	20.65	2.61	0.03	0.9	120	(28.7)	(0.64)		(< 22)	EC1(c)	C
	10 41 40.55	49 57 27.2	4.6	19.62	.58	-0.08	0.9	820	116	0.85	22.0	26.0	Q	Y
	10 42 09.71	45 49 47.8	8.5	19.93	1.16	0.28	-0.7	710	(91.3)	(0.92)		(< 17)	QC	C
N	10 42 09.91	41 30 16.5	2.4	21.52	2.77	0.60	6.7	130	(14.5)	(0.98)		< 5	EC1	F
	10 42 22.76	49 03 53.0	3.4	20.02	.24	-0.08	0.7	200	26	0.89		2.0	Q	Y
N	10 42 22.36	39 16 20.8	9.6	20.25	2.49	-0.70	17.2	380	(50.5)	(0.91)		< 6	M	F
N	10 42 28.99	39 20 21.2	9.9	20.81	2.08	-0.45	25.7	540	(76.3)	(0.88)		55.0	M	F
	10 42 53.0	41 24 57	1.9	18.54	.60	0.02	1.1	1580	245	0.81		8.5	Q	Y
	10 42 57.57	39 18 54.3	0.2	19.85	.24	0.05	-0.7	110	(14.8)	(0.90)	4.5	4.0?	Q	y
N	10 43 00.78	48 32 34.7	5.8	18.52	1.85	0.51	4.2	100	(19.3)	(0.74)		(< 27)	EC2	C‡
	10 43 12.7	42 38 18	2.0	20.57	1.68	0.10	-0.4	350	66	0.73		3.1	Q	Y
	10 43 20.58	45 27 54.1	6.5	18.67	.73	-0.05	-0.1	360	42	0.94	22.4	19.0	QC	Y
	10 43 59.23	48 43 13.9	3.2	20.45	2.34	-0.06	1.7	100	(38.9)	(0.42)		(< 21)	G	C‡
	10 44 13.24	44 32 32.1	0.9	19.68	.87	0.02	-0.1	350	57	0.79	5.1	29.0	G/OC2	Y
R	10 44 13.24	44 32 32.1	0.8	19.77	.83	-0.04	0.2	350	57	0.79	5.1	29.0	Q	Y
	10 44 22.08	41 46 00.8	5.4	18.67	.61	0.03	-0.5	140	38	0.57	29.0	14.0	QC	Y
	10 44 34.38	48 51 21.1	4.0	19.88	.77	-0.10	1.0	170	58	0.47	43.4	9.4	Q/OC1	Y
	10 44 35.76	47 41 22.4	1.7	18.48	.88	-0.10	1.1	2000	(789)	(0.42)		0.6	Q	P
S	10 44 35.76	47 41 22.4	9.8	20.30	1.77	-0.43	9.2	2000	(789)	(0.42)		0.6	M	P
	10 45 08.13	48 18 12.7	9.6	20.35	1.53	-0.14	0.7	90	(19.4)	(0.69)		(< 25)	EC2(c)	C‡
	10 45 09.35	49 55 19.8	7.7	19.76	.52	-0.09	-1.9	100	(24.3)	(0.64)		(20.6)	?(c)	C‡
S	10 45 09.35	49 55 19.8	7.8	21.00	3.55	1.20	-6.4	100	(24.3)	(0.64)		(20.6)	M	C‡
N	10 45 11.75	48 35 42.5	2.6	10.83	.90	-0.18	-1.0	90	(12.0)	(0.90)		(< 31)	?(c)	C‡
	10 45 16.88	38 53 26.8	8.1	17.58	.35	0.08	-1.2	200	35	0.76	5.7	18.0	Q	Y
N	10 45 30.78	42 16 56.5	9.1	20.23	2.14	-0.10	-9.5	450	(40.8)	(1.08)		(36.0)	EC1	C
N	10 45 59.60	46 43 56.7	6.2	21.18	3.11	-0.01	-2.9	310	(63.4)	(0.71)		(31.5)	EC2(c)	C
	10 46 00.47	46 29 09.6	3.0	20.68	3.08	-0.21	-5.7	1290	(128.3)	(1.04)		(40.9)	S	C
N	10 46 14.00	44 56 47.8	7.5	21.40	2.77	0.35	15.3	150	(22.3)	(0.86)		(30.4)	EC1	C
N	10 46 22.32	46 27 26.8	5.1	19.72	2.29	-0.51	-5.5	220	(21.9)	(1.04)		(< 20)	EC1	C
	10 46 31.93	46 11 42.6	1.8	18.52	.47	-0.08	-0.6	500	63	0.90	5.1	29.0	Q	Y
N	10 46 40.30	45 01 36.3	5.5	21.07	2.59	0.60	1.1	300	(63.6)	(0.70)		(51.6)	EC1	C
	10 46 55.3	50 09 07	0.5	20.08	1.03	0.17	-7.6	290	40	0.87		67.0	QC	Y
N	10 48 20.64	47 00 12.7	1.3	18.82	1.99	-0.18	-0.4	930	(321.0)	(0.48)		1.5	EC1(c)	P
N	10 49 04.97	39 21 00.1	9.0	20.47	3.01	0.29	-11.3	80	(12.4)	(0.81)		(67.3)	OC1	C‡
	10 49 30.41	47 50 16.9	6.2	20.80	.81	-0.04	0.6	220	41	0.73	25.8	5.0	QC	Y
	10 49 34.13	47 37 16.9	0.7	19.60	.94	-0.07	0.7	140	23	0.78	3.0	20.0	Q	Y
N	10 49 39.37	45 40 14.8	7.4	21.35	1.61	0.78	22.8	100	(26.3)	(0.60)		(41.8)	?	C‡
	10 49 39.78	48 55 58.1	7.7	17.83	.64	0.74	-4.2	120	23	0.73	2.2	33.0	M	y
	10 50 01.46	46 03 46.7	5.3	18.68	.68	0.44	-6.2	150	(23.6)	(0.83)		(22.0)	Q/EC1	n
	10 50 07.81	43 18 52.4	6.5	18.50	1.17	-1.25	-6.7	170	37	0.67	4.1	34.0	G	y
N	10 51 01.42	42 47 12.1	3.2	21.14	2.25	0.24	2.7	160	(21.4)	(0.90)		(39.9)	OC2(c)	C
	10 51 15.45	47 30 39.8	5.8	21.07	2.99	0.34	-0.4	120	(22.5)	(0.75)		(24.6)	EC2(c)	C
S	10 51 15.45	47 30 39.8	7.6	20.49	2.48	0.11	9.2	120	(22.5)	(0.75)		(24.6)	M	C
	10 51 38.56	45 57 51.9	3.8	19.19	.37	-0.01	0.1	350	49	0.86	49.0	1.5	Q	Y
	10 52 17.03	46 32 17.0	4.7	20.03	2.31	0.45	13.5	130	(18.0)	(0.89)		(46.8)	OC1	C
N	10 52 17.13	46 36 53.9	7.8	21.20	2.71	-3.36	-13.3	840	(49.4)	(1.27)		(35.8)	?	C ^j
N	10 53 00.43	47 15 47.6	8.1	20.40	2.53	-0.02	0.4	120	(28.2)	(0.65)		(35.6)	EC1(c)	C

Table 1. (cont).

(1)	(2)	(3)	(4)	(5)	(6)	(7)	(8)	(9)	(10)	(11)	(12)	(13)	(14)	(15)
	RA(1950)	Dec(1950)	r	O	$O - E$	Δ RA	Δ Dec	S_{151}	S_{1490}	α_{151}^{1490}	S_{core}	θ	Opt	
*	10 53 18.00	44 43 18.1	20.1	19.51	.30	-0.08	0.8	370	100	0.57	55.0	29.0	OC2(c)	y
S	10 53 18.00	44 43 18.1	7.0	19.66	.89	-2.00	4.5	370	100	0.57	55.0	29.0	M	y
S	10 53 18.00	44 43 18.1	5.5	19.70	.71	-2.03	13.7	370	100	0.57	55.0	29.0	M?	y
N	10 53 29.14	48 42 06.3	8.1	21.46	2.80	1.00	10.8	120	(28.6)	(0.64)		(23.6)	EC1	C
	10 53 33.44	49 36 43.0	9.1	20.30	.97	0.00	1.8	110	(12.8)	(0.97)		(< 32)	?(c)	C ^j
	10 53 52.3	49 49 43	6.3	20.94	1.54	0.05	2.2	1030	130	0.90		24.0	QC	Y
	10 54 25.55	46 12 18.2	4.2	19.59	.52	0.00	-0.5	130	13	1.01	2.0	17.0	Q/OC2	y
	10 55 17.75	49 55 40.0	2.4	18.73	.76	-0.07	1.3	1250	243	0.71		3.0	Q	L
N	10 56 51.38	48 25 07.4	2.9	20.78	3.14	0.26	4.5	100	(26.6)	(0.59)		(20.5)	EC1(c)	C†
N	10 57 25.22	46 27 08.0	0.7	20.05	1.23	-0.07	1.5	670	(177.3)	(0.60)		(< 18)	EC1	C
	10 58 32.56	49 06 38.6	2.7	20.66	.98	-0.03	1.4	250	40	0.80	7.7	23.0	Q	Y
N	10 59 15.24	47 59 36.1	9.5	18.10	2.11	1.02	-13.2	100	(10.4)	(1.02)		(< 37)	?	C†
	10 59 58.3	48 20 02	1.8	20.31	.97	-0.11	0.7	210	42	0.70		28.0	QC	Y
	11 00 37.65	46 30 10.9	6.1	18.97	.72	-0.17	-1.6	180	(52.6)	(0.55)		(20.7)	Q	C ^j
	11 00 48.33	46 06 19.4	7.9	20.20	1.19	0.62	-6.9	140	(13.9)	(1.04)		(43.4)	?	C ^l
N	11 01 25.07	44 59 20.5	3.9	21.35	3.70	-0.08	-1.0	110	(14.7)	(0.90)		(< 29)	EC1(c)	C
	11 01 33.79	49 44 35.5	2.1	20.06	1.34	-0.09	2.2	870	211	0.62	211.0	0.1	QC	L
N	11 01 52.03	47 43 05.8	6.5	20.47	3.55	-0.82	-3.2	400	(87.4)	(0.68)		(44.3)	EC1	C
	11 02 50.23	46 35 40.8	2.3	20.93	2.35	-0.02	0.1	220	(40.2)	(0.76)		(< 20)	?(c)	C ^r
N	11 07 53.72	48 03 22.8	2.3	19.10	2.47	-0.15	-1.3	880	(122.6)	(0.89)		(67.8)	EC1(c)	C

Table 1. (cont).

(1)	(2)	(3)	(4)	(5)	(6)	(7)	(8)	(9)	(10)	(11)	(12)	(13)	(14)	(15)
	RA(1950)	Dec(1950)	r	O	$O - E$	ΔRA	ΔDec	S_{151}	S_{1490}	α_{151}^{1490}	S_{core}	θ	Opt	
	09 53 27.30	41 00 44.7	12.4	21.06	1.51	-0.06	-0.2	260	66	0.60	35.0	11.0	QC	Y
	09 54 55.71	44 20 23.7	10.4	19.47	0.56	-0.10	2.0	1480	212	0.85	7.0	16.0	Q	y
	09 55 33.1	42 32 29	5.8	18.46	1.26	0.65	-6.6	520	(72.2)	(0.89)		39.0	M	y
	10 00 00.23	41 02 44.0	10.8	20.17	0.88	-0.05	0.4	130	23	0.76	8.0	24.0	Q	Y
	10 03 51.64	45 10 16.1	10.2	17.35	0.10	-0.66	3.8	1500	222	0.83	77.0	7.7	M	Y
	10 04 53.6	48 40 04	9.9	20.24	1.35	1.05	5.5	300	42	0.86		11.3	M	y
	10 05 47.68	46 27 44.2	14.6	15.37	0.75	1.59	24.1	880	144	0.79	2.0	54.0	M	Y
	10 07 26.09	41 47 25.5	13.5	16.21	0.24	-0.02	0.7	8300	(1236)	(0.86)	153.0	33.0	Q	S
	10 09 21.46	40 44 24.2	10.3	19.56	1.36	-0.67	-2.0	130	13	1.01		3.5	M	y
	10 10 24.61	36 10 25.1	11.1	20.72	1.63	-1.36	-8.2	120	10	1.09	10.0	0.5	M	N
	10 13 01.12	47 23 10.2	7.8	19.63	3.18	-0.07	0.0	300	41	0.87	1.4	20.0	G	y
	10 15 28.8	38 20 32	10.4	17.93	0.21	-0.09	-3.3	1200	(274)	(0.66)		43.0	Q	V
	10 15 52.81	48 23 37.1	11.5	20.52	1.15	-0.63	-6.5	120	18	0.83	18.0	0.9	M	Y
	10 17 08.68	43 38 51.8	13.8	20.01	1.11	-0.57	-4.4	120	26	0.67	26.0	0.6	M	N
	10 19 03.37	41 41 14.4	9.5	14.85	0.09	0.24	-10.2	430	195	0.35	154.0	4.5	M	y
	10 20 28.96	44 29 26.0	10.0	17.93	0.58	0.07	2.1	160	(27.6)	(0.79)	12.0	(19.9)	Q	N
R	10 20 28.96	44 29 26.0	10.7	18.44	0.32	-0.06	0.4	160	(27.6)	(0.79)	12.0	(19.9)	Q	N
R	10 20 28.96	44 29 26.0	11.5	17.80	0.62	-0.09	1.7	160	(27.6)	(0.79)	12.0	(19.9)	Q	N
	10 23 30.75	35 40 27.0	14.9	20.85	1.36	-0.32	-11.7	230	(23.7)	(1.02)		16.0	M	F
	10 24 13.69	34 57 33.1	11.4	19.52	1.33	0.63	-5.6	120	(25.4)	(0.70)		(67.4)	M	n
	10 32 02.14	39 26 14.1	5.1	18.47	1.01	-0.15	-1.5	190	30	0.81	1.2	42.0	Q	y
	10 32 41.85	34 48 48.2	7.1	17.37	0.56	0.06	-3.4	160	(19.0)	(0.96)		(< 22)	G	C
	10 34 16.66	44 43 46.9	11.0	20.25	1.03	-0.26	-12.7	280	43	0.82	17.7	9.4	M	y
	10 35 56.22	37 45 02.1	11.5	17.86	0.42	0.11	0.7	210	(55.4)	(0.60)	17.5	70.0	Q	F
	10 38 08.37	40 21 27.2	10.1	21.37	1.65	1.44	-11.8	170	22	0.89	0.5	10.0	M	Y
	10 43 25.80	46 08 50.3	11.6	20.39	0.84	-1.32	-7.3	250	(28.3)	(0.98)		(51.8)	?	C ^j
	10 54 24.25	45 36 19.8	10.4	20.48	1.20	0.13	-2.6	110	(13.9)	(0.93)		(< 25)	EC1	C
	11 03 07.88	47 49 23.2	14.9	18.25	1.32	-0.10	-15.5	730	(93.8)	(0.92)		(14.8)	?	C ^j

Table 2. Table summarising the radio and optical properties of the subsidiary sample of candidate 7CQ quasars. Format is the same as Table 1 with additional references for Column 15: S, Reid et al. (1995) and Owen & Puschell (1984).

3 RADIO OBSERVATIONS

The observations were made on 1990 April 14, 17 and 19, and 1991 August 2 with the VLA in A-array, using two IFs of bandwidth 50 MHz at a mean frequency of 1.49 GHz. Two 4-min snapshots, separated by roughly 2 hr, were made of each source. The flux density calibrator was 3C 286 for which a flux density of 14.5 Jy was assumed.

The data were calibrated in the standard way at the VLA. Subsequent reduction was carried out using the AIPS package. Where possible, after initial mapping and cleaning, the data were self-calibrated once for phase. The Gaussian restoring beam on the full-resolution maps was circular with a FWHM of 1.4 arcsec; lower resolution maps, for which the FWHM of the restoring beam was 4 arcsec, were made in every case to look for larger-scale structure. The flux densities, positions and sizes of compact features were measured from the maps by fitting a Gaussian to them using the AIPS task IMFIT; the flux densities of more extended features were estimated using TVSTAT.

For A-array at 1.49 GHz the VLA is intrinsically insensitive to structure with angular scale above 38 arcsec, a value which may be compromised somewhat by the incomplete UV-coverage of our snapshot observations; bandwidth smearing also limits the accuracy of the maps at distances of > 30 arcsec from the pointing centre. Some of the sources observed here have structures on these scales, and we have utilised the 1.4-GHz NVSS survey (Condon et al. 1998) to recover reliable flux densities in these cases.

4 RESULTS

The results of our observations are summarised in Table 1 (for the main sample) and Table 2 (for the subsidiary sample); radio maps of the extended sources in these two samples are shown in Fig. 3. The optical position of each quasar candidate was examined in relation to the high resolution radio map; as a result a substantial number were rejected as candidates because their APM positions (which should be accurate to better than 1 arcsec) were significantly offset from any plausible site for a jet-producing nucleus. The compact features on the VLA maps have a positional accuracy of about ± 0.3 arcsec. Further spectroscopic observations of the remainder (Paper II) were carried out to determine whether or not they were quasars. Details of the current status of each object are given in Tables 1 & 2.

Figure 3. 1.49 GHz VLA maps of the extended sources. Peak brightnesses and contour levels are given in units of mJy beam⁻¹; negative contours are shown dashed. A cross marks the APM position of the quasar candidate. The hatched ellipse shows the FWHM of the Gaussian restoring beam. 0953+410: peak 34.1; contours $0.4 \times (-1, 1, 2, \dots, 5, 10, \dots, 25, 50, 75)$. 0954+443: peak 139; contours $1 \times (-1, 1, 2, \dots, 5, 10, \dots, 25, 50, \dots)$. 0955+425: peak 5.0; contours $0.5 \times (-1, 1, 2, \dots)$. 0955+428: peak 36.8; contours $0.5 \times (-1, 1, 2, \dots, 5, 10, \dots, 20, 40, \dots)$. 0958+413: peak 30.1; contours $0.4 \times (-1, 1, 2, \dots, 5, 10, \dots, 25, 50, 75)$. 0958+423: peak 35.1; contours $0.4 \times (-1, 1, 2, \dots, 5, 10, \dots, 25, 50, 75)$. 0959+408: peak 2.4; contours $0.3 \times (-1, 1, 2, \dots)$. 0959+401: peak 23.0; contours $0.4 \times (-1, 1, 2, \dots, 5, 10, \dots, 25, 50)$. 1000+410: peak 7.9; contours $0.4 \times (-1, 1, 2, \dots, 5, 10, 15)$. 1001+425: peak 48.0; contours $0.5 \times (-1, 1, 2, \dots, 5, 10, 15, 20, 40, 60, 80)$. 1001+408: peak 37.5; contours $0.4 \times (-1, 1, 2, \dots, 5, 10, \dots, 25, 50, 75)$. 1003+451: peak 83.3; contours $0.8 \times (-1, 1, 2, \dots, 10, 20, \dots)$.

Figure 3. (cont). 1004+486: peak 22.0; contours, $0.4 \times (-1, 1, 2, \dots, 5, 10, \dots)$. 1005+455: peak 5.9; contours $0.5 \times (-1, 1, 2, \dots)$. 1005+464: peak 52.9; contours $0.7 \times (-1, 1, 2, \dots, 10, 20, \dots)$. 1006+471: peak 16.8; contours $0.4 \times (-1, 1, 2, \dots, 5, 10, \dots)$. 1007+385: peak 13.9; contours $0.4 \times (-1, 1, 2, \dots, 5, 10, \dots)$. 1009+407: peak 4.0; contours $0.6 \times (-1, 1, 2, \dots)$. 1009+369 (4-arcsec beam): peak 9.2; contours $0.5 \times (-1, 1, 2, \dots, 5, 10, 15)$. 1009+369 (1.4-arcsec beam): peak brightness 5.2; contours $0.4 \times (-1, 1, 2, 3, 6, \dots)$. 1009+361 (4-arcsec beam): peak 25.0; contours $1.4 \times (-1, 1, 2, \dots, 5, 10, \dots)$. 1009+385: peak 3.3; contours $0.3 \times (-1, 1, 2, \dots)$. 1010+420: peak 7.1; contours $0.4 \times (-1, 1, 2, \dots, 5, 10, \dots)$.

Figure 3. (cont) 1011+414: peak 36.7; contours $0.5 \times (-1, 1, 2, \dots, 5, 10, \dots, 20, 40, 60)$. 1011+446: peak 4.4; contours $0.25 \times (-2, -1, 1, 2, 3, 4, 6, \dots)$. 1011+496: peak 332; contours $2 \times (-1, 1, 2, \dots, 5, 10, \dots, 25, 50, \dots)$. 1012+326: peak 19.3; contours $0.8 \times (-1, 1, 2, \dots, 5, 10, \dots)$. 1012+403: peak 8.5; contours $0.4 \times (-1, 1, 2, \dots, 5, 10, 15, 20)$. 1013+473: peak 1.3; contours $0.25 \times (-1, 1, 2, \dots)$. 1013+366: peak 45.8; contours $0.5 \times (-1, 1, 2, \dots, 5, 10, \dots, 20, 40, \dots)$. 1014+464: peak 17.4; contours $0.5 \times (-1, 1, 2, \dots, 5, 10, \dots)$. 1014+442: peak 11.3; contours $0.5 \times (-1, 1, 2, 4, \dots)$. 1015+463: peak 18.8; contours $0.5 \times (-1, 1, 2, 4, 8, \dots)$. 1015+359: peak 556; contours $1 \times (-1, 1, 2, \dots, 10, 20, \dots, 100, 200, \dots)$. 1015+436: peak 25.3; contours $0.8 \times (-1, 1, 2, \dots, 5, 10, \dots)$.

Figure 3. (cont) 1015+483: peak 13.2; contours $0.5 \times (-1, 1, 2, \dots, 5, 10, \dots)$. 1018+456: peak 46.8; contours $0.4 \times (-1, 1, 2, \dots, 10, 20, \dots)$. 1018+407: peak 28.5; contours $0.8 \times (-1, 1, 2, \dots, 5, 10, \dots)$. 1018+327: peak 53.0; contours $1 \times (-1, 1, 2, \dots, 5, 10, \dots)$. 1019+416: peak 153; contours $0.8 \times (-1, 1, 2, \dots, 5, 10, \dots, 25, 50, \dots)$. 1019+372: peak 25.8; contours $0.5 \times (-1, 1, 2, \dots, 5, 10, \dots)$. 1019+378: peak 10.0; contours $0.4 \times (-1, 1, 2, \dots, 5, 7.5, \dots)$. 1019+459: peak 22.1; contours $0.4 \times (-1, 1, 2, \dots, 5, 10, \dots)$. 1019+397: peak 39.7; contours $1 \times (-1, 1, 2, \dots, 5, 10, \dots)$. 1019+341: peak 6.0; contours $1 \times (-1, 1, 2, \dots)$. 1020+481: peak 424; contours $1.5 \times (-2, -1, 1, 2, \dots, 6, 12, \dots, 30, 60, \dots)$. 1020+486: peak 31.0; contours $0.4 \times (-1, 1, 2, \dots, 10, 15, \dots)$.

Figure 3. (cont) 1021+398: peak 6.8; contours $1 \times (-1, 1, 2, \dots)$. 1022+393: peak 17.2; contours $1 \times (-1, 1, 2, 3, 4, 8, \dots)$. 1022+435: peak 5.0; contours $0.4 \times (-1, 1, 2, \dots 5, 10)$. 1024+419 (4-arcsec beam): peak 30.5; contours $0.6 \times (-1, 1, 2, \dots 10, 20, \dots)$. 1024+419 (1.4-arcsec beam): peak 20.0; contours $0.4 \times (-1, 1, 2, \dots 10, 20, \dots)$. 1024+467: peak 14.1; contours $0.4 \times (-1, 1, 2, \dots 5, 10, \dots)$. 1024+483: peak 156; contours $1.5 \times (-1, 1, 2, \dots 10, 20, \dots)$. 1024+431: peak 8.2; contours $0.4 \times (-1, 1, 2, \dots 5, 10, \dots)$. 1024+362: peak 5.6; contours $0.8 \times (-1, 1, 2, \dots)$. 1025+433: peak 12.6; contours $0.5 \times (-1, 1, 2, \dots 5, 10, \dots)$. 1027+326: peak 90.1; contours $0.6 \times (-1, 1, 2, \dots 5, 10, \dots 25, 50, \dots)$. 1027+434: peak 34.5; contours $0.5 \times (-1, 1, 2, \dots 5, 10, \dots 20, 40, 60)$. 1027+340: peak 3.8; contours $0.3 \times (-1, 1, 2, \dots)$.

Figure 3. (cont) 1028+415: peak 23.9; contours $0.5 \times (-1, 1, 2, \dots 5, 10, \dots)$. 1028+421: peak 30.7; contours $0.4 \times (-1, 1, 2, \dots 5, 10, \dots 25, 50, 75)$. 1029+498: peak 21.5; contours $0.5 \times (-1, 1, 2, \dots 5, 10, \dots)$. 1029+378: peak 36.1; contours $0.4 \times (-1, 1, 2, \dots 5, 10, \dots 25, 50, 75)$. 1029+394: peak 6.5; contours $0.4 \times (-1, 1, 2, \dots)$. 1030+415: peak 486; contours $0.4 \times (-1, 1, 2, \dots 5, 10, \dots 50, 150, 250, \dots)$. 1031+497: peak 6.2; contours $0.6 \times (-1, 1, 2, \dots)$. 1032+394: peak 4.4; contours $0.3 \times (-1, 1, 2, \dots)$. 1032+454: peak 5.8; contours $0.3 \times (-1, 1, 2, \dots 5, 10, 15)$. 1032+343: peak 43.1; contours $0.6 \times (-1, 1, 2, \dots 5, 10, \dots 25, 50)$. 1032+444: peak 23.4; contours $0.4 \times (-1, 1, 2, \dots 5, 10, \dots)$. 1032+382: peak 44.5; contours $0.4 \times (-1, 1, 2, \dots 5, 10, \dots 25, 50, \dots)$.

Figure 3. (cont) 1033+483: peak 51.2; contours $0.6 \times (-1, 1, 2, \dots, 5, 10, \dots, 25, 50, \dots)$. 1034+461A: peak 3.0; contours $0.3 \times (-1, 1, 2, \dots)$. 1034+461B: peak 1.2; contours $0.4 \times (-1, 1, 2, 3)$. 1034+461C: peak 0.8; contours $0.3 \times (-1, 1, 2)$. 1034+470: peak 51.0; contours $0.5 \times (-1, 1, 2, \dots, 5, 10, \dots, 20, 40, \dots)$. 1034+447: peak 16.4; contours $0.4 \times (-1, 1, 2, \dots, 5, 10, \dots)$. 1035+389: peak 5.5; contours $0.4 \times (-1, 1, 2, \dots)$. 1035+486: peak 31.4; contours $0.5 \times (-1, 1, 2, \dots, 10, 20, \dots)$. 1035+500: peak 23.1; contours $0.4 \times (-1, 1, 2, \dots, 5, 10, \dots)$. 1037+426: peak 7.6; contours $0.5 \times (-1, 1, 2, \dots, 5, 10, 15)$. 1037+450: peak 6.4; contours $0.5 \times (-1, 1, 2, \dots)$.

Figure 3. (cont) 1038+403: peak 3.2; contours $0.4 \times (-1, 1, 2, \dots)$. 1038+432: peak 31.2; contours $0.4 \times (-1, 1, 2, \dots 5, 10, \dots 25, 50, 75)$. 1038+468: peak 21.2; contours $0.4 \times (-1, 1, 2, \dots 5, 10, \dots)$. 1041+499: peak 21.5; contours $0.6 \times (-1, 1, 2, \dots 10, 15, \dots)$. 1042+490: peak 10.5; contours $0.4 \times (-1, 1, 2, \dots 5, 10, \dots)$. 1042+414: peak 79.2; contours $0.5 \times (-1, 1, 2, \dots 5, 10, \dots 20, 40, \dots)$. 1042+393: peak 4.4; contours $1 \times (-1, 1, 2, \dots)$. 1043+426: peak 54.8; contours $0.4 \times (-1, 1, 2, \dots 5, 10, \dots 25, 50, \dots)$. 1043+454: peak 21.8; contours $0.4 \times (-2, -1, 1, 2, \dots 5, 10, \dots)$. 044+445: peak 12.7; contours $0.3 \times (-1, 1, 2, \dots 5, 10, \dots)$.

Figure 3. (cont) 1044+417 (1.4-arcsec beam): peak 26.8; contours $0.3 \times (-1, 1, 2, \dots 5, 10, \dots 30, 60, \dots)$. 1044+417 (4-arcsec beam): peak 28.2; contours $0.7 \times (-1, 1, 2, \dots 5, 10, \dots)$. 1044+488: peak 42.7; contours $0.5 \times (-1, 1, 2, \dots 10, 20, \dots)$. 1045+388: peak 8.9; contours $0.3 \times (-1, 1, 2, \dots 5, 10, \dots)$. 1046+461: peak 11.4; contours $0.4 \times (-1, 1, 2, \dots 5, 10, \dots)$. 1046+501: peak 4.1; contours $0.3 \times (-1, 1, 2, \dots 5, 10, \dots)$. 1049+478: peak 25.2; contours $0.4 \times (-1, 1, 2, \dots 5, 10, \dots)$. 1049+476: peak 3.9; contours $0.4 \times (-1, 1, 2, \dots)$. 1049+489: peak 2.3; contours $0.5 \times (-1, 1, 2, \dots)$.

Figure 3. (cont) 1050+433 (4-arcsec beam): peak 4.5; contours $0.6 \times (-1, 1, 2, \dots)$. 1050+433 (1.4-arcsec beam): peak 4.0; contours $0.3 \times (-1, 1, 2, \dots)$. 1051+459: peak 30.3; contours $0.4 \times (-1, 1, 2, \dots, 5, 10, \dots)$. 1053+447: peak 53.0; contours $0.4 \times (-1, 1, 2, \dots, 10, 20, \dots)$. 1053+498: peak 46.4; contours $0.6 \times (-1, 1, 2, \dots, 10, 20, \dots)$. 1054+462: peak 3.5; contours $0.25 \times (-1, 1, 2, \dots)$. 1058+491: peak 7.6; contours $0.4 \times (-1, 1, 2, \dots)$. 1059+483: peak 10.9; contours $0.5 \times (-1, 1, 2, \dots, 5, 10, \dots)$.

4.1 Notes on individual sources

0954+443 (Table 2) The APM position is 2 arcsec south of the radio component which seems likely to be the core. The optical object has, however, been confirmed as a quasar — the origin of this unusually large radio/optical offset will be discussed in Paper II.

0955+425 (Table 2) This is not included in the final version of the 7C/APM cross-matched list because the optical object was re-classified as non-stellar on both the *E* and *O* POSS-I plates.

1004+486 (Table 2) This is not part of the final version of the 7C/APM cross-matched list because the optical object was re-classified as non-stellar on both the *E* and *O* POSS-I plates.

1009+407 (Table 2) There are two stellar objects in the field of this source one of which, detailed in Table 1, is coincident with the radio peak. The original 7C/APM cross-match picked up the other stellar object (which is detailed in Table 2).

1009+361 (Table 1) There are three radio sources in this field (with a maximum separation of 264 arcsec) of which the central one is coincident with a quasar. The two other sources are significantly affected by bandwidth smearing on our VLA map but are, at most, only slightly resolved. There is no evidence for any structure linking the three sources on the 151-MHz map of the area, or on either our VLA map or the FIRST map. Inspection of the NVSS map does show some evidence for low-level bridge emission connecting the core to the component to the south-west, but although the three components do lie roughly on a straight line, there is as yet no unambiguous evidence that all three are related.

1013+473 (Table 2) This is not included in the final version of the 7C/APM cross-matched list because the optical object was re-classified as non-stellar on both the *E* and *O* POSS-I plates; this object has been confirmed as a galaxy by optical spectroscopy (paper II).

1019+416 (Table 2) This is not included in the final version of the 7C/APM cross-matched list because the optical object was re-classified as non-stellar on the *E* POSS-I plate, and was confused on the *O* plate.

1019+378 (Table 1) The position of the stellar object is 2.5 arcsec south of the radio component which seems likely to be the core; further astrometric and spectroscopic work is required to confirm whether this object is really associated with the source.

1022+435 (Table 1) There is some diffuse structure to the east of the core which has not been adequately mapped by our VLA observations. We have therefore preferred to tabulate the flux density at 1.4 GHz from the NVSS survey.

1024+419 (Table 1) The low-resolution map shows possible low-brightness wings extending away from the axis of the source. The tabulated 1.4-GHz NVSS

flux density significantly exceeds the value ($S_{1490} = 76$ mJy) estimated from our map.

1024+349 (Table 2) The source was classified as extended (40 arcsec) in 7C; no definite extended structure was detected by our VLA observations but comparison with the NVSS data shows that this is simply because the surface brightness is too low. Extended structure is clearly apparent in the FIRST map. The original stellar object can be rejected on positional grounds; however there is a very faint ($E = 19.7$) optically-unresolved object coincident with the peak of the source on our VLA map (RA 10 24 13.69, DEC 34 57 33.1), but this object is too red to appear on the *O* plate and may be a galaxy.

1028+415 (Table 1) There is marginal evidence for a faint extension ~ 2 arcsec in p.a. 315° although it remains possible that this is an artefact of imperfect calibration.

1029+498 (Table 1) The most easterly of the three bright regions in the southern component seems most likely to be the core on positional grounds since the other radio sub-components are more than 3 arcsec from the optical position.

1032+394 (Table 2) The position of the optical object (which the APM analysis finds to be extended on both the *E* and *O* POSS-I plates) is 1.7 arcsec east and 1.4 arcsec north of that of the core; further astrometric and spectroscopic work is required to confirm whether this object is really associated with the source.

1034+461 (Table 1) There are three radio sources in this field; there is no evidence that any of these are associated with the stellar object.

1034+447 (Table 2) The original candidate ID can be rejected on positional grounds (it is not shown on the radio map). The cross shows the position of a very faint ($O = 21.8$) object detected only on the *O* POSS-I plate (RA 10 34 16.55, DEC 44 43 49.4); it lies close to the northernmost peak of the radio source and is a plausible, but not compelling, optical ID.

1042+393 (Table 1) There is a possible very weak component 10 arcsec east of the core; however the map is of poor quality and, especially as there is no corresponding feature on the FIRST map, it may not be real. The flux density from the NVSS survey is preferred in Table 1.

1049+489 (Table 1) The noise on this map is high because of residual sidelobe emission from a bright source about 4 arcmin to the south-west of the 7C radio source, and it is thus not clear whether the component in the north-east of the map is real. There are two stellar objects on the POSS-I *E* plate near to the 7C source. The brightest of these is a redshift $z = 0.478$ quasar known in the literature as 5C2.10, but a comparison of our APM finding chart and the optical image of the field presented by Ellingson & Yee (1994) shows that the position they give for this quasar (RA 10 49 41.00, Dec 48 55 53.0) is in error, and that our new APM position (10 49 39.06,

48 56 01.9) should be preferred. Moreover, our radio map shows that this quasar is not likely to be the true ID of the 7C (and 5C) radio source; this quasar, which lies in a rich cluster, should be re-designated as a radio-quiet object. There is a second stellar object which is significantly closer to the radio core position ($\Delta\text{RA} = 0^{\text{s}}03$, $\Delta\text{Dec} = 1.4$ arcsec). It has an E magnitude of 19.1 but is not visible on the O plate so that $O - E > 2.4$. It corresponds to Object 391 of Ellingson & Yee who failed to secure a redshift for it so it is not yet clear whether the radio source is identified with a spatially-compact galaxy, which may be in the same cluster as the known quasar, or whether it is a background or foreground quasar with an unusually red colour. The radio source was also detected in B-array VLA observations at 1.4 GHz by Hutchings et al. (1996).

1050+460 (Table 1) This candidate was omitted from the VLA programme because the optical object was classified as non-stellar on the E POSS-I plate; subsequent spectroscopy (paper II) has revealed that this object is nevertheless a quasar.

1050+433 (Table 1) The original candidate ID can be rejected on positional grounds. There is, however, a galaxy with an E magnitude of 14.7 coincident with the core of this radio trail source ($\Delta\text{RA} = -0^{\text{s}}02$, $\Delta\text{Dec} = 0.0$ arcsec).

1053+447 (Table 1) It is not clear whether the compact source to the north-west whose radio position is given in Table 1 is related to the extended source in the south-east. There are three optical objects in the field which may be related; their positions, O magnitudes, and colours ($O - E$) are as follows:

A	10 53 18.08	44 43 17.3	19.51	0.30
B	10 53 20.00	44 43 13.6	19.66	0.89
C	10 53 20.03	44 43 04.4	19.70	0.71

Object A, which is stellar on the E plate and confused on the O plate, is very close to the peak of the compact source and is a good ID for this component, and possibly all the radio structure. Object B is stellar on both plates but appears to be unrelated to any of the radio emission. Object C, which is extended on the E plate and stellar on the O , lies close to one of the bright peaks in the extended source, and is a plausible separate ID for the extended source in the south-east.

5 THE 7CQ SAMPLE AND SELECTION EFFECTS

Full discussion of the 7CQ sample is left to future papers. We concentrate here on analysing the possible effects of the selection criteria outlined in Section 2. We exclude from this discussion the 21 radio sources with $S_{151} \leq 0.1$ Jy since these lie below our adopted radio flux density limit. We also exclude ob-

jects which are associated with other types of optical object, namely the 5 confirmed galaxies (category ‘G’) and the one BL Lac object (‘BL’), and radio sources for which any proposed APM ID can be rejected on positional grounds (the 40 objects in category ‘M’) and/or spectroscopic grounds (the 9 proposed IDs which turned out to be stars, ‘S’).

This leaves the following objects in Tables 1 and 2: 70 confirmed quasars (‘Q’); 27 quasar candidates, i.e., objects verified as good optically-unresolved IDs which currently lack spectroscopic confirmation (‘QC’); 13 objects which are optically unresolved but which are not yet verified as good IDs, and which in addition lack optical spectra (‘?’); and 36 objects which are optically unresolved on only one of the two POSS-I plates (categories ‘EC1’, ‘EC2’, ‘OC0’, ‘OC1’ and ‘OC2’). The sky positions of these objects are shown in Fig. 4. Taking category ‘Q’ and ‘QC’ objects together as our 7CQ sample we will argue that any further missing quasars constitute only a small and unbiased fraction of those meeting well-defined radio and optical flux density criteria over the sky region delineated in Fig. 4.

5.1 Radio-loud quasars missing from Tables 1 and 2

We consider here ways in which radio-loud quasars above the S_{151} limit may have been excluded from Tables 1 and 2.

First, we investigate the imposition of an r cutoff during our sample selection. A simple statistical analysis shows why this selection criterion was a practical necessity. Data from the final APM analysis were used to assess the probability of a random coincidence between a radio source and a stellar object in a particular colour range. The surface density of random objects was estimated by assuming that the objects with r greater than 20 arcsec are, indeed, chance associations. The results are summarised in Table 3 which lists the observed numbers and those expected by chance with r in the range 0–5, 5–10 and 10–15 arcsec, expressed as a function of APM colour ($O - E$) in the range <1 , 1–2, 2–3 and >3 (see O & E rows in Table 3). It can be seen that there are significant numbers of true associations amongst the objects with $O - E < 1$ even out to 15 arcsec. However, for the redder objects the proportion of chance associations increases rapidly. It is clear from this analysis that, if we wish to obtain a sample of SSQs which lacks a strong colour bias, whilst at the same time avoiding excessive numbers of random associations, we should select samples of objects with an r cutoff of at most 10 arcsec. This was the motivation behind our original survey, and our first set of VLA follow-up observations. It then became clear (as discussed in Section 5.2) that red objects could be excluded with little risk of excluding quasars, and we therefore constructed a subsidiary sample of candidates with $10 < r < 15$ arcsec and

Figure 4. The sky locations of the following objects from Tables 1 and 2 with $S_{151} > 100$ mJy (see Table 1 caption for full details of these categories): confirmed quasars ('Q' – filled circles); candidate quasars ('QC' – open circles); possible quasars ('?' – open triangles); and objects which have a non-stellar APM category on one plate ('EC1', 'EC2', 'OC0', 'OC1', 'OC2' – open squares). The sky coverage of the individual POSS-I plate pairs are illustrated by the rectangular boxes.

blue optical colours. Information on these objects can be found in Table 2.

Fig. 5 suggests that we are not missing a significant number of quasars with $r > 10$ arcsec. The evidence from our subsidiary 7CQ sample (e.g. objects in Table 2) is that there are very few, although not zero, quasars with $r > 10$ arcsec, but that the number drops off so rapidly with r that very few are expected with $r > 15$ arcsec. It is extremely difficult to model this source of incompleteness because the value of r is likely to be a complicated function of S_{151} (due to increasing inaccuracy in the 7C position at fainter val-

ues of S_{151}), and the internal structure of the source — specifically on how well the low-resolution low-frequency position matches the position of the compact radio nucleus. Note the discussion of 1053+447 in Section 4.1 as an example of the difficulties that can be involved. At the $S_{151} > 0.5$ Jy level the dominant contribution is from 'real' offsets as the random errors in 7C position are $\lesssim 2$ arcsec (McGilchrist et al. 1990). The results of the 7C Redshift Survey (Willott et al. 1998b) provide empirical evidence that $\ll 10$ per cent of this population have real offsets which are large enough to cause problems: all 18 SSQs in this *com-*

$O - E$	< 1	1-2	2-3	> 3	Total
Radio-optical separation 0–5 arcsec					
Observed $O \& E$	51	26	14	7	98
Expected $O \& E$	2	11	10	3	26
Observed O	10	40	0	0	50
Expected O	1	28	0	0	29
Observed E	0	16	31	4	51
Expected E	0	12	14	2	28
Radio-optical separation 5–10 arcsec					
Observed $O \& E$	31	40	28	10	109
Expected $O \& E$	7	33	30	8	78
Observed O	12	80	0	0	92
Expected O	3	84	0	0	87
Observed E	0	28	32	11	71
Expected E	0	34	40	5	79
Radio-optical separation 10–15 arcsec					
Observed $O \& E$	24	60	47	11	142
Expected $O \& E$	11	55	49	13	128
Observed O	14	133	2	0	149
Expected O	8	142	2	0	152
Observed E	0	55	55	8	118
Expected E	0	58	68	8	134

Table 3. Statistics of the observed radio-optical separations in comparison with matches expected from random associations between radio sources and objects categorised as stellar by the APM analysis. Objects detected on both O and E plates are considered separately from those detected on just one of the plates. In this latter case we have determined colours by assuming that the object lies just below the magnitude limit of the plate on which it is not detected by the APM analysis.

plete survey (with a flux density limit $S_{151} > 0.5$ Jy) have $r < 10$ arcsec. In absolute terms the largest real offsets are likely to occur for the quasars with the largest radio angular sizes, which will themselves tend to be in the high flux density samples. However, even amongst the 41 quasars with $S_{151} > 12$ Jy in the revised 3C sample (Laing et al. 1983) there are none for which $r > 10$ arcsec. That there are likely to be very few quasars with very large angular sizes in the 7CQ sample is further confirmed by the work of Dingley (1990). He searched for the optical counterparts of radio-faint ($0.4 \leq S_{151} \leq 1.0$ Jy), large angular size ($1.5 \leq \theta \leq 3$ arcmin) sources across 0.33 sr of the 7C survey (including almost all of the 7CQ area shown in Fig. 4). VLA and optical spectroscopic follow-up (Dingley 1990; Cotter, Rawlings & Saunders 1996) has shown that the areal density of quasars obeying these radio criteria (and with optical magnitudes above the POSS-I limits) is $\lesssim 10$ sr $^{-1}$, and few if any are therefore expected in the 7CQ sample. At the lowest flux densities ($100 \leq S_{151} \leq 200$ mJy) the effects of the random positional errors will dominate over the real offsets. The standard errors in the positions at

these flux density levels are in the range 5–10 arcsec (Pooley, Waldram & Riley 1998). The search radius of 10 arcsec can then be as much as one standard deviation so that up to 33 per cent of the quasars could lie outside this range. This potential source of incompleteness must be taken into account alongside the decreasing fraction of the 7CQ area which is complete to the faintest S_{151} levels (see Fig. 2). Because the positional errors are random this can be treated as an additional decrease in the effective area of the 7CQ survey at $S_{151} \lesssim 200$ mJy.

A second way in which quasars may be missing from Tables 1 and 2 results from our insistence that quasar candidates be detected on both the O and E POSS-I plates — a question inextricably linked with the limiting optical magnitude of the 7CQ survey. We adopted this selection criterion because of the large number of 7C/APM cross-matches in which the object appeared on only one of the plates; a summary of the numbers involved is included in Table 3. Such objects are optically faint and lie close to the magnitude limit of the plates on which they were detected. The areal density of such objects is high, and as a consequence there is a high chance that a given association is simply a chance projection. Nevertheless, inspection of Table 3 shows that there is still a significant number of genuine IDs on just the E plate. However, since these objects have to be red [$(O - E) > 1.5$] to avoid detection on the O plate, most and possibly all are probably radio galaxies, and we will not consider them further; the reasons for this will be discussed in Section 5.2. The 7C/APM cross-matches amongst objects detected optically on just the O plate is also well above the number expected by chance. These blue IDs *will* include a significant number of genuine radio-loud quasars. We have not yet followed up these objects either with the VLA or spectroscopically. Although missing from Tables 1 and 2, the existence of these quasars does not affect the completeness of the 7CQ sample provided a magnitude of $E \approx R \approx 20$ is adopted as the appropriate optical limit for the survey.

5.2 Radio-loud quasars amongst objects in Tables 1 and 2 but not followed-up

We consider here selection effects arising from incomplete VLA and optical follow-up of the objects in Tables 1 and 2. To illustrate this discussion we plot in Fig. 6 the E magnitude versus the $O - E$ colour for all objects in these tables.

The confirmed quasars all have colours bluer than $(O - E) \approx 1.8$ as do 25 of the 27 objects in the ‘QC’ category. Only 5 of the 13 objects which lack VLA/optical follow-up (category ‘?’) have colours bluer than this limit, so we can achieve a good level of formal completeness simply by adding this colour selection criterion. We will henceforth refer to the 25 blue ‘QC’ objects plus the other 11 blue objects (5 in

Figure 5. The angular separation r between the 7C radio source position and the APM optical position plotted against the total 7C flux density. The filled circles represent confirmed quasars (category ‘Q’), the open circles, candidate quasars (category ‘QC’) and the stars, steep-spectrum quasars from the flux-limited 7C Redshift Survey (Willott et al. 1998b). Very few quasars lie above the dotted line which shows the r cutoff used in the original 7CQ sample.

category ‘?’ and 6 in one of the ‘EC/OC’ categories) as the 36 unconfirmed quasar candidates. We shall argue in this section that this additional colour criterion excludes few if any quasars.

First, we will discuss the objects which the APM analysis finds to be optically resolved on either or both of the plates. Ideally this procedure should reject quasar-like objects only if they are of low optical luminosity and lie at low redshift ($z \ll 0.5$) because only then can an optically-extended host galaxy contribute significantly to the light. In this case the only quasars to be missed would be those whose optical luminosities are lower than the lu-

minosity of a giant galaxy: these systems are normally termed N-galaxies, or broad-line radio galaxies, rather than quasars (Peacock, Miller & Longair 1986; Willott et al. 1998b). However, the existence of 11 spectroscopically-confirmed quasars in Table 1 (and in Fig. 6) which the APM analysis categorised as not having simple unresolved optical structure on one of the plates indicates that some quasars would have been missed if the APM classification had remained unquestioned. The origin of this problem is the breakdown of the APM classification algorithm, particularly (as illustrated by the faint E magnitudes of the quasars ‘resolved’ by the APM analysis) for ob-

Figure 6. The APM E magnitude plotted against the $O - E$ colour for the following categories of object: filled circles, confirmed quasars (category ‘Q’ in Tables 1 & 2); open circles and open triangles, candidate quasars which are secure optical identifications (category ‘QC’) or insecure optical identifications (category ‘?’) respectively; open squares, objects classified as extended on one of the POSS-I plates (a union of the EC1, EC2, OC0, OC1, OC2 categories defined in Table 1). The dashed lines show the effective $E \approx 20$ and $O - E \approx 1.8$ limits of the 7CQ sample, although we argue in Section 5.2 that only the former leads to a significant loss of radio-loud quasars from the sample. These lines divide the plot into quadrants: objects detected only on the E plate would fill out the top region of the bottom-right quadrant; and objects detected only on the O plate would lie in the top-left quadrant. In the bottom-left quadrant there are 25 ‘QC’ objects, 5 ‘?’ objects and 7 ‘EC/OC’ objects, and therefore 37 unconfirmed quasar candidates remaining in the 7CQ sample.

jects near the magnitude limits of the POSS-I plates. We thus attempted where possible to obtain VLA and spectroscopic follow-up of the fainter objects in which APM classification was in doubt; only a few faint blue candidates were not followed up. The majority of the objects in the ‘EC/OC’ categories are resolved on the E plate and are bright enough in E that the APM classification is likely to be reliable; they have red

$O - E$ colours just as one expects for low-redshift objects in which stellar light dominates. It is also possible that some genuinely point-like quasars are spuriously classified as extended by the APM analysis; evidence that this can happen is provided by the source 0955+425 in Table 2 which was identified as point-like by the first version of the APM classification analysis (see Section 2) but which was classified as extended

on both POSS-I plates by the second version. The number of cases which have been missed completely is likely to be very small given that it requires inaccurate classification on both plates, and by both versions of the APM analysis; these hypothetical objects would be likely to have unusual properties (for example being projected close to a foreground star or galaxy) which would render them difficult cases for any automated classification.

Second, we consider the 13 objects excluded from any follow-up (either with the VLA or spectroscopically), namely those in category ‘?’ in Tables 1 and 2. These were excluded from follow-up either because of large 7C angular size (1 case), red optical colour (5 cases), or for random reasons (7 cases). We have already argued that excluding either red objects or large angular size radio sources is unlikely to reject quasars. Since the remaining objects were excluded randomly, these exclusions should not bias the sample significantly.

Although we have followed up stellar objects regardless of colour from four of the five POSS-I plate pairs we have not yet found any 7C quasars with red colours [$(O - E) > 1.8$]. Inspection of Fig. 6 shows that only two 7CQ objects are optically unresolved, have red colours ($O - E > 1.8$) and currently lack spectroscopic follow-up. Even if both of these are red quasars, they would constitute only a small ($\ll 10$ per cent) fraction of the population. This is a direct consequence of two effects: first, the low fraction of lightly-reddened and/or intrinsically red quasars in samples selected at low radio frequency (Willott et al., 1998a, and in prep.); and second, the tiny areal density expected for quasars at such high redshifts that their Ly α line becomes redshifted beyond the peak in the O -plate sensitivity.

5.3 Concluding remarks

The discussion in Sections 5.1 and 5.2 highlights an extremely important problem which is an ineluctable consequence of any survey for radio quasars which employs the POSS-I plates as the means of making optical identifications. The depth of these plates is insufficient to identify all the quasars associated with a sample of 7C radio sources. Indeed, the majority of the radio-loud quasars above the S_{151} limit will probably lie at magnitudes fainter than the POSS-I limits. The most direct indication of this comes from the optical magnitude distribution of the quasars, predominantly SSQs, in the 7C Redshift Survey (Willott et al. 1998b): in this survey optical spectra were taken of *all* objects with $S_{151} > 0.5$ Jy in two patches of sky together covering 0.013 sr, and secure redshifts are now available for ≈ 90 per cent of the sample (Blundell et al. 1998; Rawlings et al. 1998; Willott et al. 1998a). Just over 50 per cent of the quasars in this $S_{151} > 0.5$ Jy sample are bright enough optically to be seen on either the O or E POSS-I plate. The cor-

relation between the radio and optical luminosities of SSQs (Serjeant et al. 1998) implies that an even lower fraction of quasars will appear on the POSS-I plates at fainter S_{151} limits. The 7CQ sample will therefore find only the optically-brightest SSQs at any redshift, and is likely to miss ≈ 60 per cent of the total number of SSQs (Willott et al. 1998b). All analyses based on the 7CQ sample must take careful account of this effect. This means that, for example, a proper assessment of the quasar fraction as a function of S_{151} is beyond the scope of the present paper. A *lower limit* on the quasar fraction (QF) in the whole 7CQ sample is given by the ratio of the total number of confirmed (category ‘Q’) quasars (70) to the total number of 7C radio sources (with $S_{151} > 0.1$ Jy) in the region covered by 7C/APM cross-match (2409 sources), namely $QF > 3$ per cent. Correcting for the unfinished spectroscopic follow-up and various other sources of incompleteness (chiefly the expectation that more than half of the radio-loud quasars fall below the magnitude limits of the POSS-I plates) could eventually yield a $QF \sim 10$ per cent. This may prove to be significantly lower than the $QF \sim 20 - 30$ per cent seen in low-frequency radio samples selected at higher limiting values of S_{151} (e.g. the 3C and 7C samples; Willott et al. 1998b).

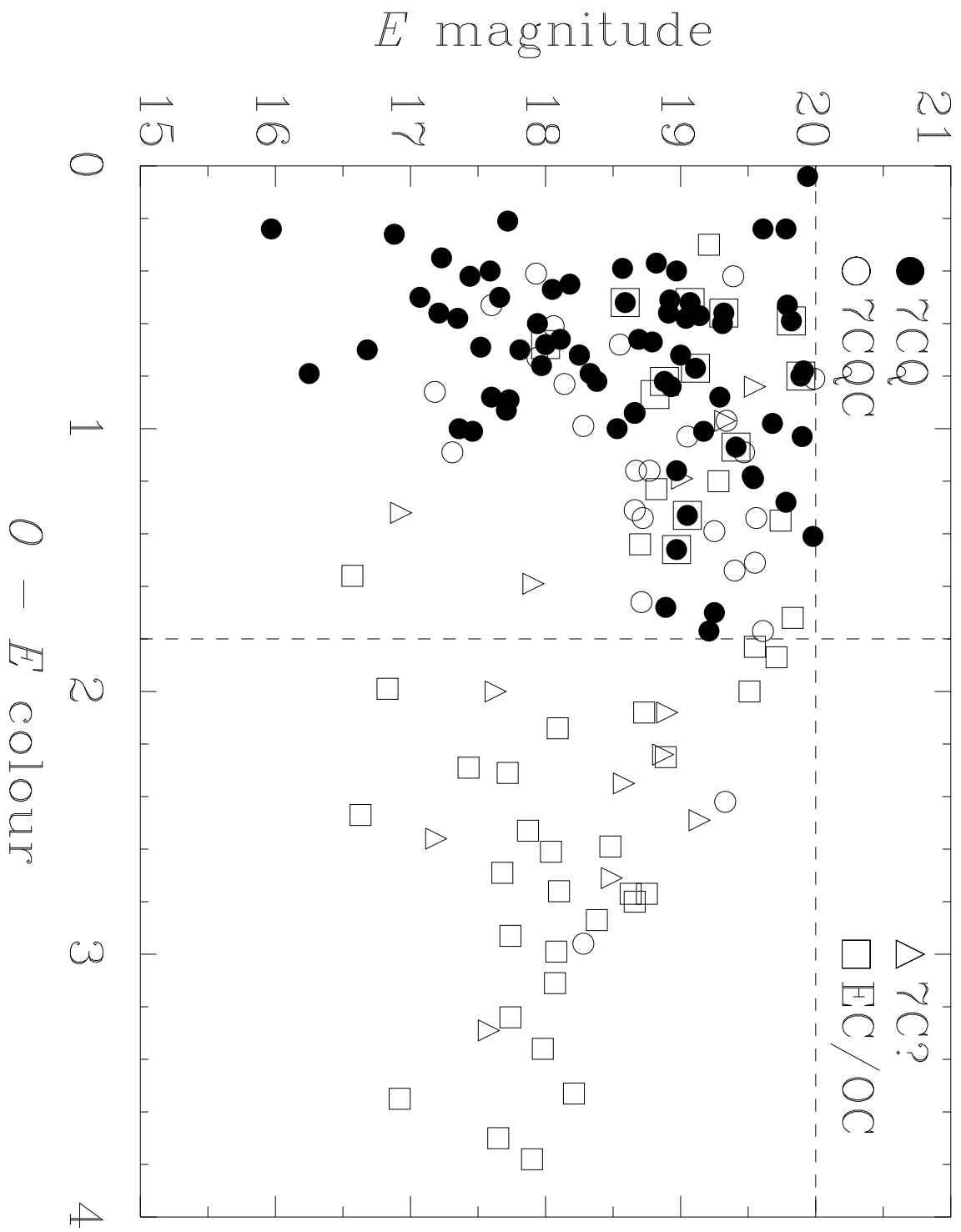
Finally we note that the problem of insufficient plate depth may severely compromise other SSQ surveys based on POSS-I IDs, e.g. the B3-VLA quasar sample (Vigotti et al. 1997). Surveys which utilise deeper optical plates (e.g. UK Schmidt plates with a limiting magnitude of $B_J \approx 22.5$), and which have brighter S_{151} selection limits — and we are thinking here specifically of the Molonglo/APM survey (MAQS; Serjeant et al. 1998, and in prep.) and the Molonglo Quasar Survey (MQS; Kapahi et al. 1998 and refs. therein) — should be far less prone to this problem. The problems introduced for SSQ surveys having dual radio and optical selection criteria are addressed quantitatively by Willott et al. (1998b).

ACKNOWLEDGEMENTS

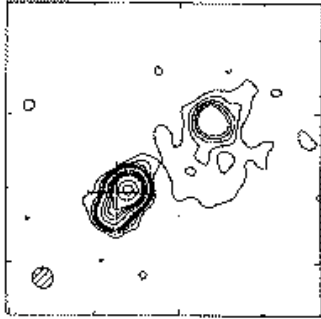
We are particularly grateful to Paul Alexander, Guy Pooley, Richard Saunders, Stephen Serjeant and Peter Warner who helped with various aspects of this work. We thank the anonymous referee for some extremely useful suggestions. We also thank the staff of the VLA. The National Radio Astronomy Observatory is operated by Associated Universities, Inc., under co-operative agreement with the National Science Foundation. This research has made use of the NASA/IPAC Extragalactic Database, which is operated by the Jet Propulsion Laboratory, Caltech, under contract with the National Aeronautics and Space Administration.

REFERENCES

- Antonucci R.R.J., 1985, ApJS, 59, 499
- Becker R.H., White R.L., Helfand D.J., 1995, ApJ, 450, 559
- Blundell K.M., Rawlings S., Riley J.M., Willott C.J., Laing R.A., 1998, to be submitted to New A.
- Condon J.J., Cotton, W.D., Greisen, E.W., Yin, Q.F., Perley, R.A., Taylor, G.B., Broderick, J.J., 1998, AJ, 115, 1693
- Cotter G., Rawlings S., Saunders R., 1996, MNRAS 281, 1081
- Dingley S.J., 1990, Ph.D. thesis, University of Cambridge
- Ellingson E., Yee H.K.C., 1994, ApJS, 92, 33
- Hutchings J.B., Gower A.C., Ryneveld S., Dewey A., 1996, AJ, 111, 2167
- Kapahi V.K., Athreya R.M., Subrahmanya C.R., Baker J.C., Hunstead R.W., McCarthy P.J., van Breugel, W., 1998, ApJS, 118, 327
- Lacy M., Riley J.M., Waldram E.M., McMahon R.G., Warner P.J., 1995, MNRAS, 276, 614
- Laing R.A., Riley J.M., Longair M.S., 1983, MNRAS, 204, 151
- Law-Green J.D.B., Leahy, J.P., Alexander, P., Allington-Smith, J.R., van Breugel, W.J.M., Eales, S.A., Rawlings, S.G., Spinrad, H., 1995, MNRAS, 274, 939
- Machalski J., Condon J.J., 1986, AJ, 91, 998
- McGilchrist M.M., Baldwin J.E., Riley J.M., Titterington D.J., Waldram E.M., Warner P.J., 1990, MNRAS, 246, 110
- Owen F.N. & Puschell J.J., 1984, AJ, 89, 932
- Patnaik A.R., Browne I.W.A., Wilkinson P.N., Wrobel J., 1992, MNRAS, 254, 655
- Peacock J.A., Miller L., Longair M.S., 1986, MNRAS, 218, 265
- Pooley D.M., Waldram E.M., Riley J.M., 1998, MNRAS, 298, 637
- Rawlings S., Blundell K.M., Lacy M., Willott C.J., Eales S.A., 1998, in *Observational Cosmology with the New Radio Surveys*, eds. M.N. Bremer et al., 171, Kluwer
- Reid A., Shone D.L., Akujor C.E., Browne I.W.A., Murphy D.W., Walsh D., 1995, A&AS, 110, 213
- Riley J.M. & Warner P.J., 1994, MNRAS, 269, 166
- Serjeant S., Rawlings S., Maddox S.J., Baker J.C., Clements D., Lacy M., Lilje P.B., 1998, MNRAS, 294, 494
- Vigotti M., Grueff G., Perley R., Clark B.G., Bridle A.H., 1989, AJ, 98, 419
- Vigotti M., Vettolani G., Merighi R., Lahulla J.F., Pedani M., 1997, A&AS, 123, 219
- Willott C.J., Rawlings S., Blundell K.M., Lacy M. 1998a, in *Observational Cosmology with the New Radio Surveys*, eds. M.N. Bremer et al., 209, Kluwer
- Willott C.J., Rawlings S., Blundell K.M., Lacy M. 1998b, MNRAS, 300, 625

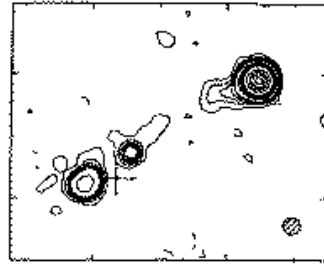


0953+410



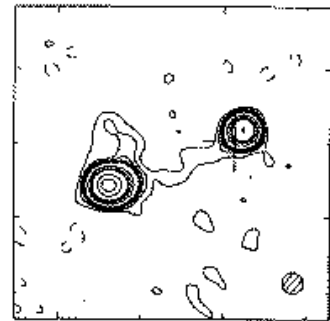
09 53 28 09 53 27

0954+443



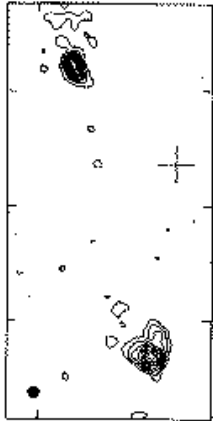
09 54 56 09 54 55

0955+428



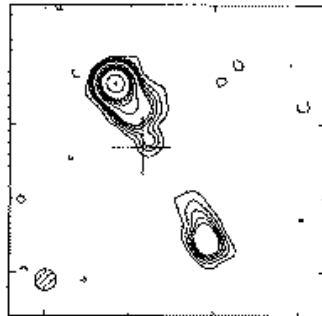
09 55 51 09 55 50

0955+425



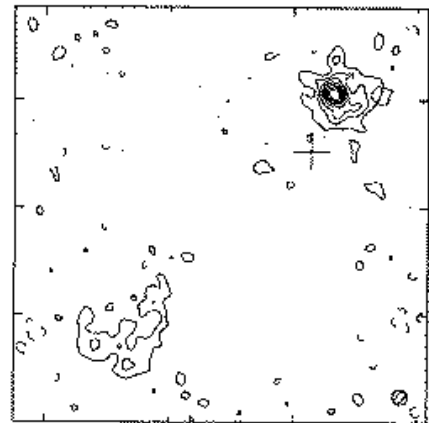
09 55 34 09 55 32

0958+413



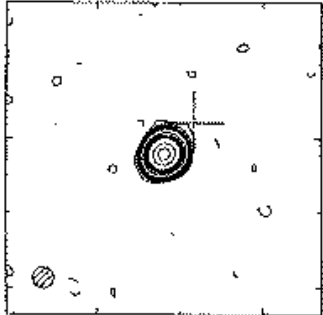
09 58 32 09 58 31

0959+408



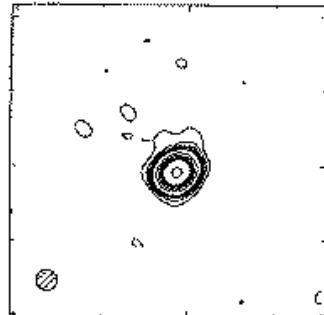
09 59 16 09 59 14

0958+423



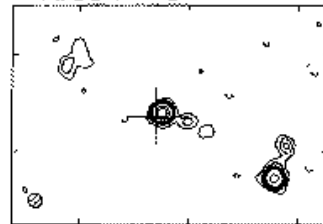
09 58 38 09 58 37

0959+401



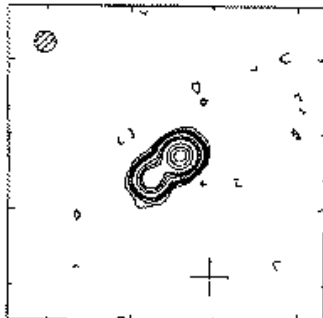
09 59 28 09 59 27

1000+410



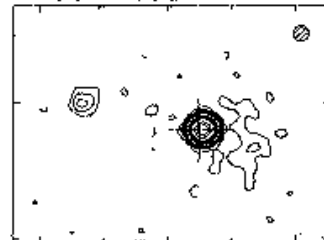
10 00 01 10 00 00 09 59 59

1001+425



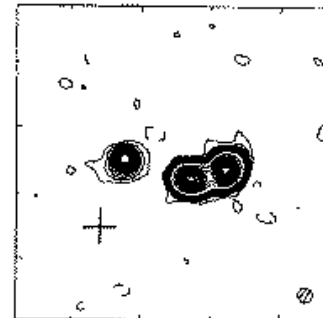
10 01 21 10 01 20

1001+408



10 01 41 10 01 40 10 01 39

1003+451



10 03 52 10 03 51

44 20 30

44 20 20

42 51 30

42 51 20

41 21 20

41 21 10

40 49 00

40 48 50

40 48 40

40 07 50

40 07 40

40 07 30

41 02 50

41 02 40

42 23 40

42 23 30

42 34 00

42 33 50

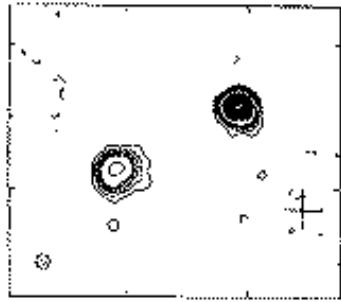
40 51 24

40 51 12

45 10 20

45 10 10

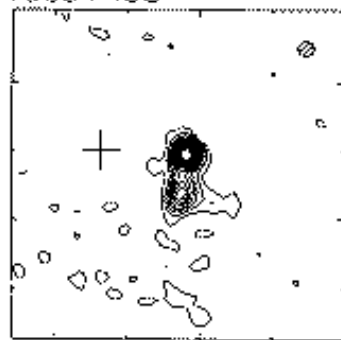
1004+486



48 40 12
48 40 00

10 04 54 10 04 53

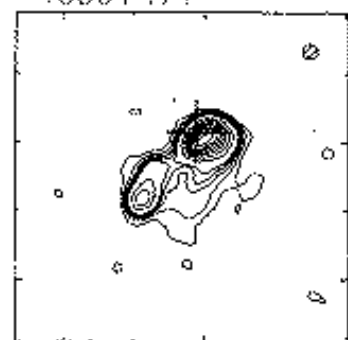
1005+455



45 33 30
45 33 20

10 05 32 10 05 31

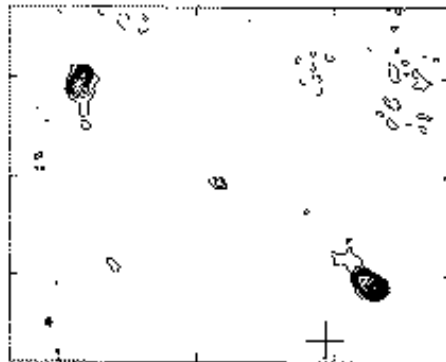
1006+471



47 10 10
47 10 00

10 06 34 10 06 33 10 06 32

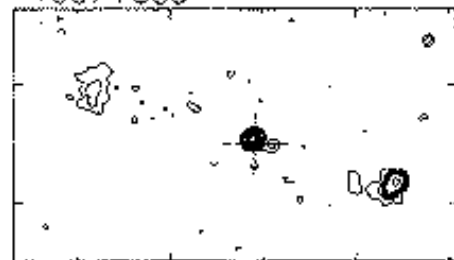
1005+464



46 28 00
46 27 45
46 27 30

10 05 50 10 05 48 10 05 46

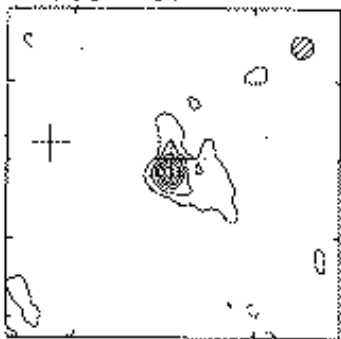
1007+385



38 32 30
38 32 15

10 08 00 10 07 58

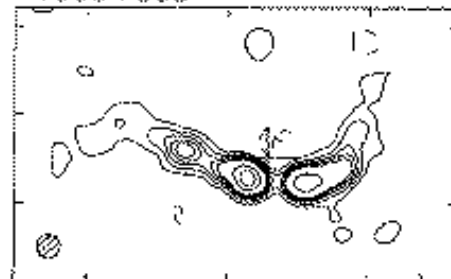
1009+407



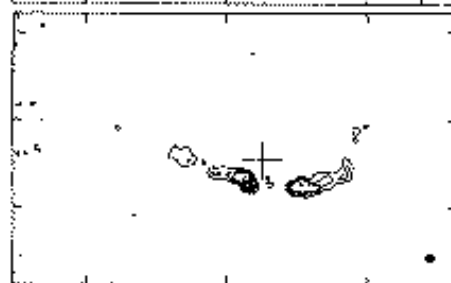
40 44 30
40 44 20

10 09 22 10 09 21

1009+369



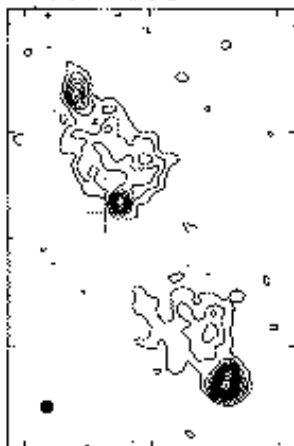
36 54 45
36 54 30
36 54 15



36 54 45
36 54 30
36 54 15

10 09 26 10 09 24 10 09 22

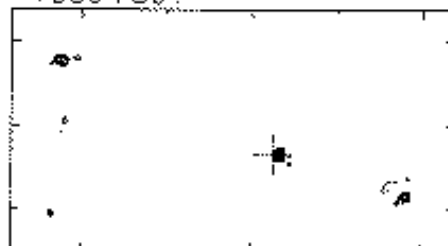
1009+385



38 34 40
38 34 20

10 09 55 10 09 54 10 09 53

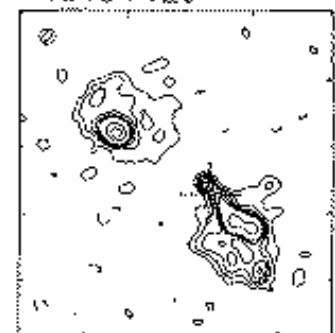
1009+361



36 10 00
36 09 00
36 08 00

10 10 00 10 09 50 10 09 40

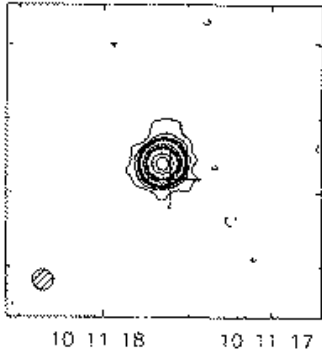
1010+420



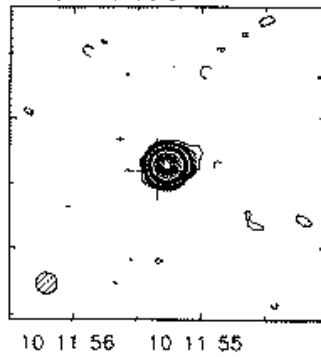
42 04 12
42 04 00

10 10 47 10 10 46

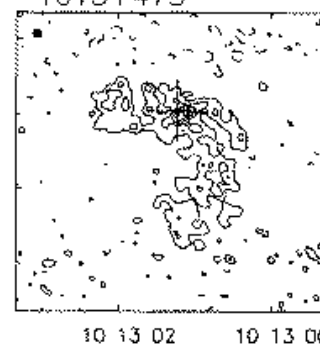
1011+414



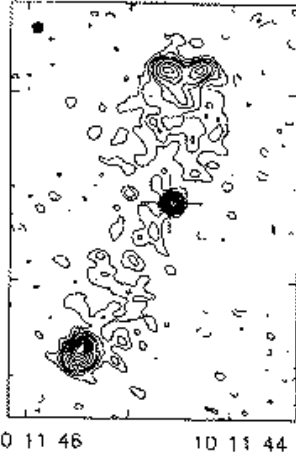
1011+496



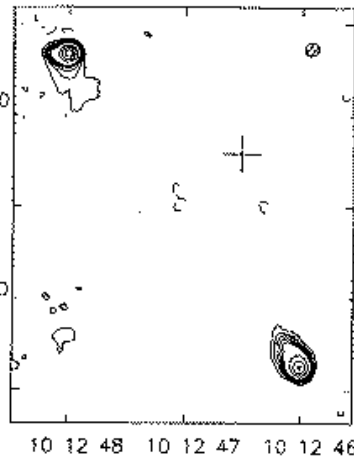
1013+473



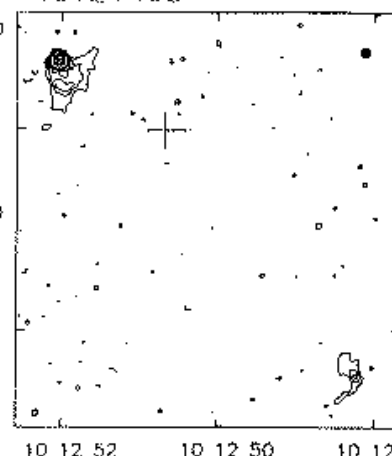
1011+446



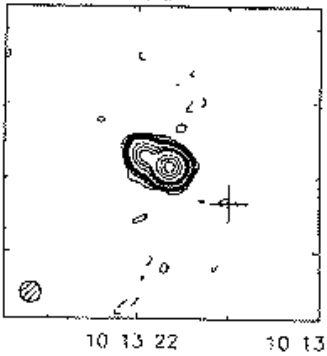
1012+326



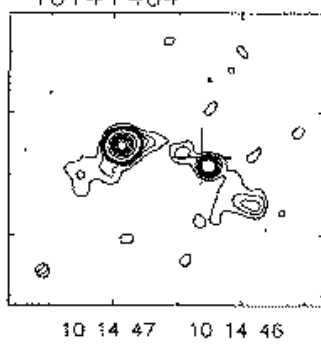
1012+403



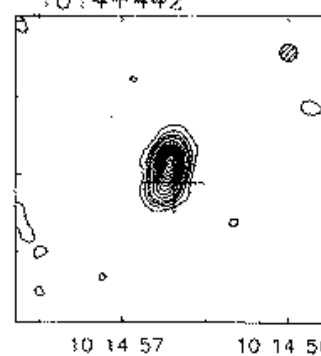
1013+366



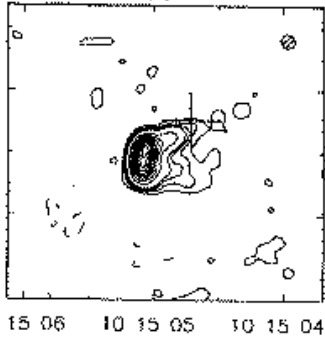
1014+464



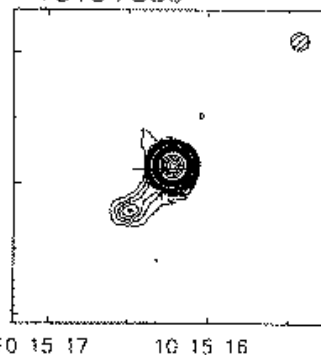
1014+442



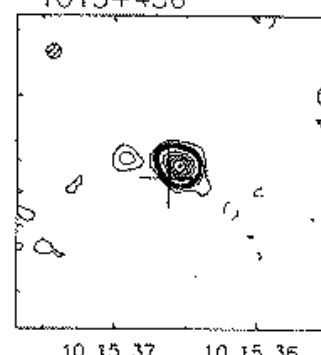
1015+463



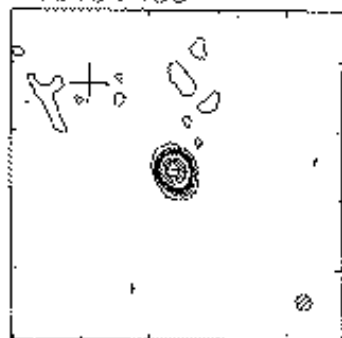
1015+359



1015+436



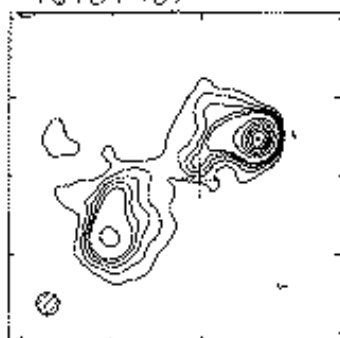
1015+483



48 23 40

48 23 30

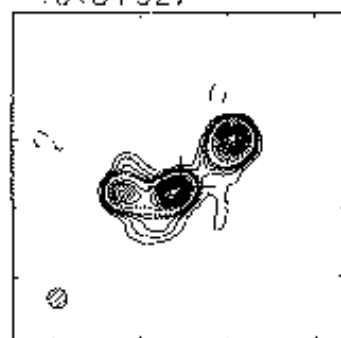
1018+407



40 47 50

40 46 50

1018+327



32 42 50

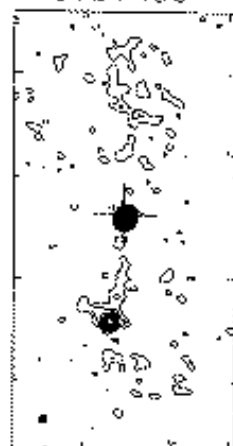
32 42 40

10 15 54 10 15 53 10 15 52

10 18 42 10 18 41

10 18 48 10 18 47

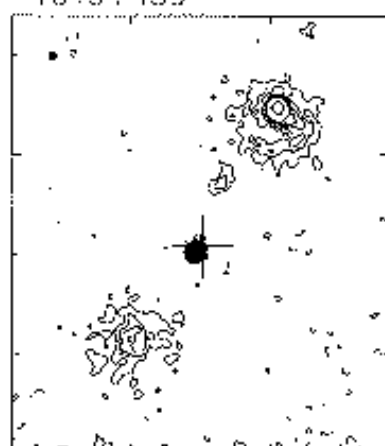
1018+455



45 39 00

45 38 30

1019+459



45 56 30

45 56 00

1019+372



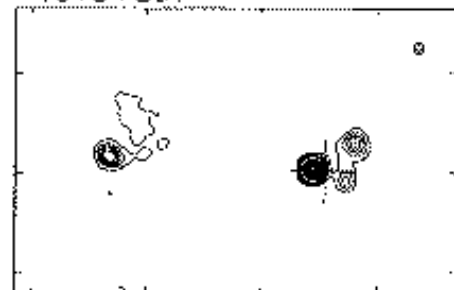
37 13 50

37 13 40

10 19 14

10 19 12

1019+397

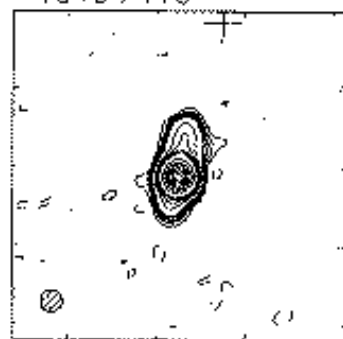


39 47 10

39 47 00

39 45 50

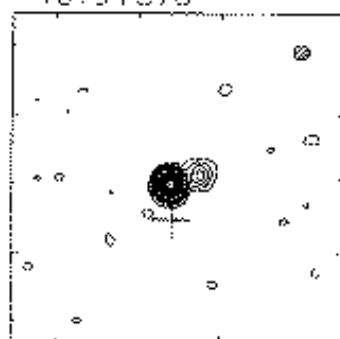
1019+416



41 41 20

41 41 10

1019+378



37 50 50

37 50 40

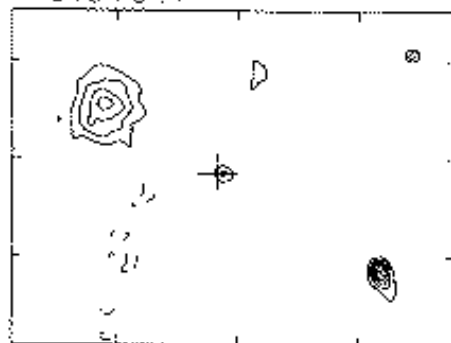
10 19 42

10 19 40

10 19 04 10 19 03

10 19 32 10 19 31

1019+341

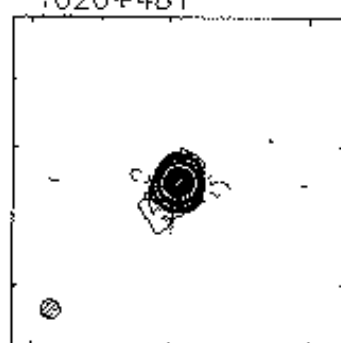


34 06 20

34 06 10

34 06 00

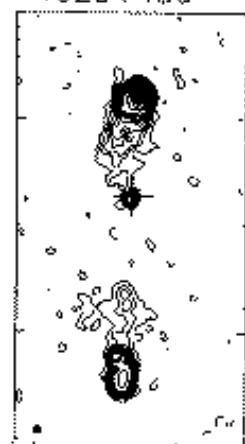
1020+481



48 07 00

48 06 50

1020+486



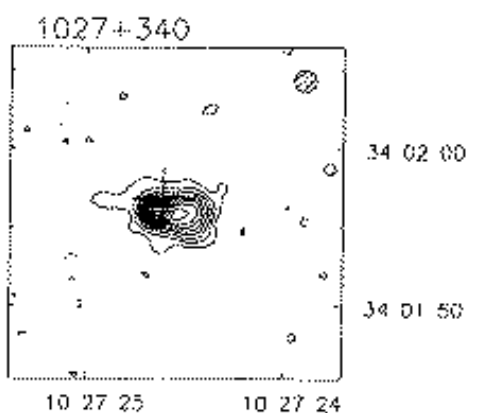
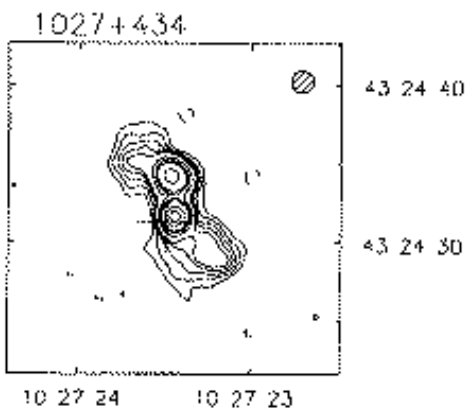
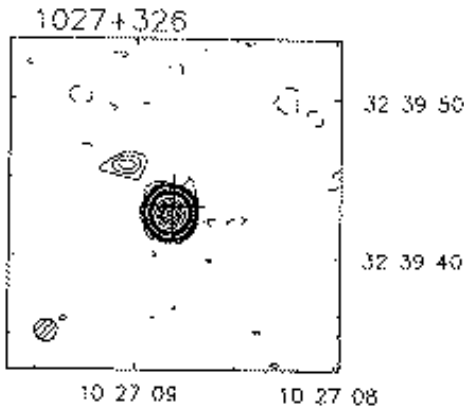
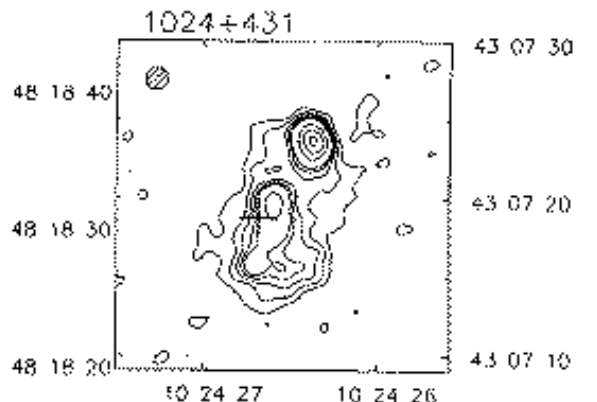
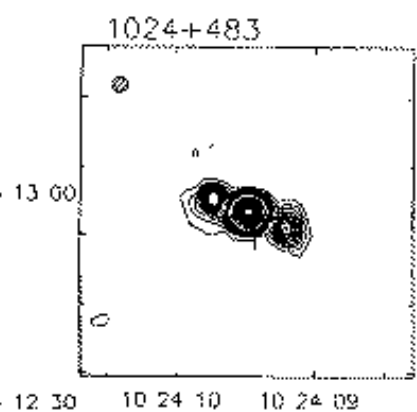
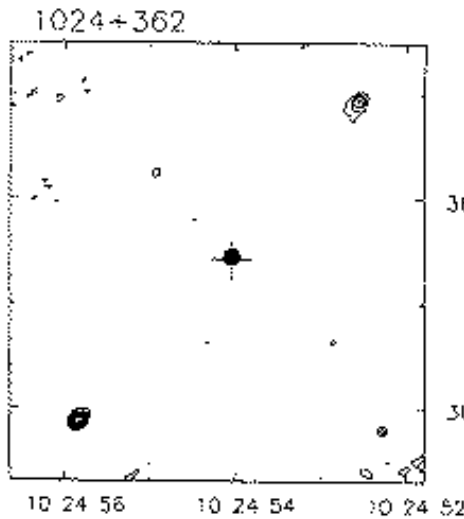
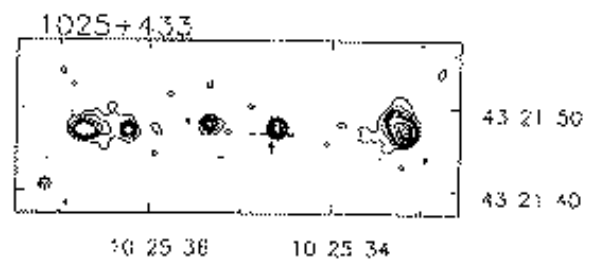
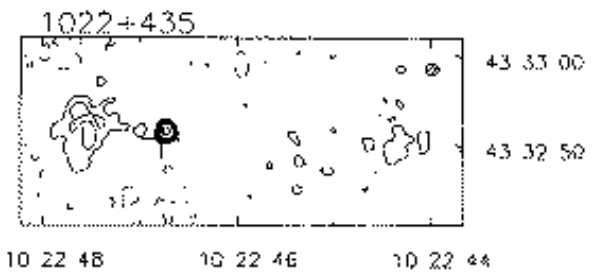
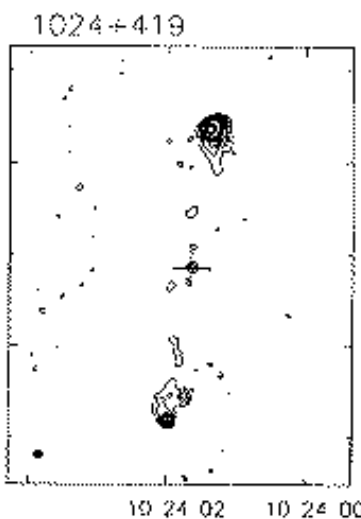
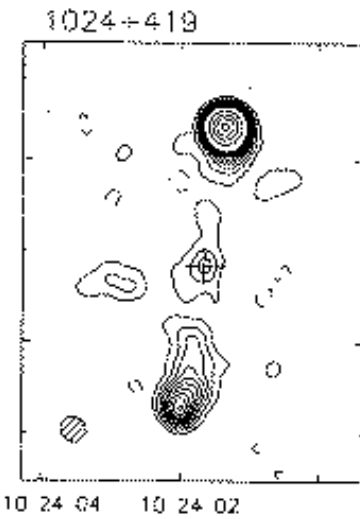
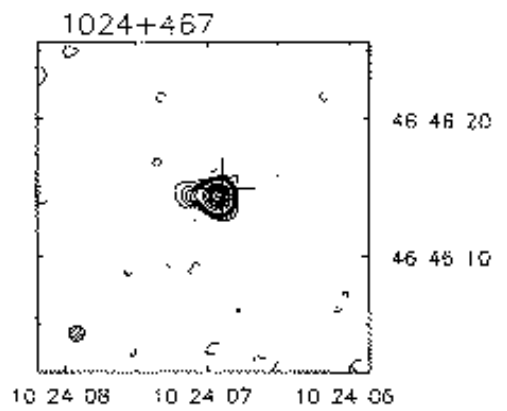
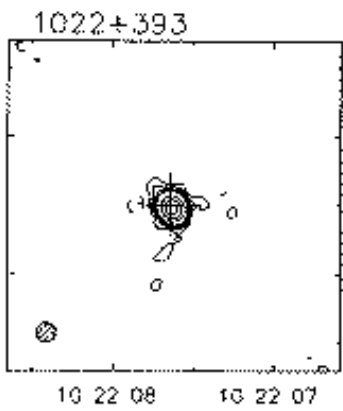
48 40 00

48 39 30

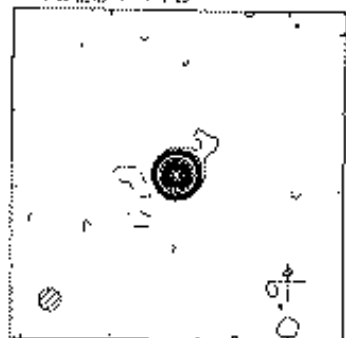
10 19 57 10 19 56 10 19 55

10 20 07 10 20 06 10 20 05

10 20 26 10 20 24



1028+415

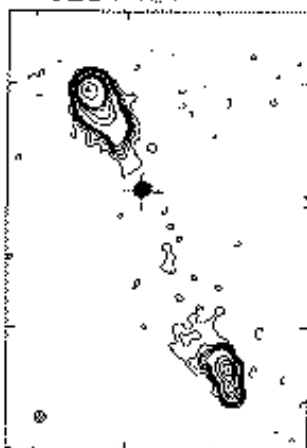


41 34 10

41 34 00

10 28 11 10 28 10

1028+421

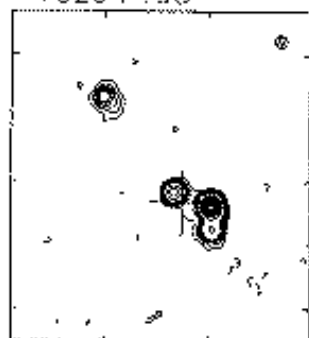


42 10 00

42 09 30

10 28 48 10 28 46

1029+498



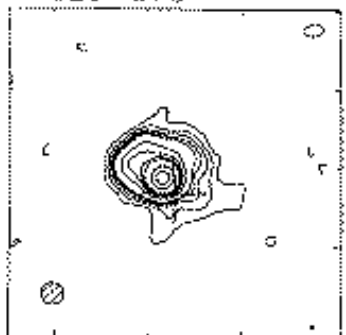
49 48 24

49 48 12

49 48 00

10 29 32 10 29 31

1029+378

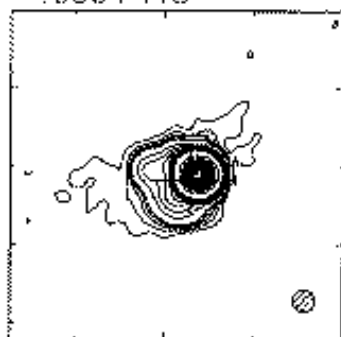


37 54 00

37 53 50

10 29 48 10 29 47

1030+415

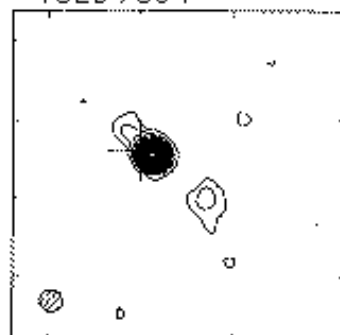


41 31 40

41 31 30

10 30 08 10 30 07

1029+394

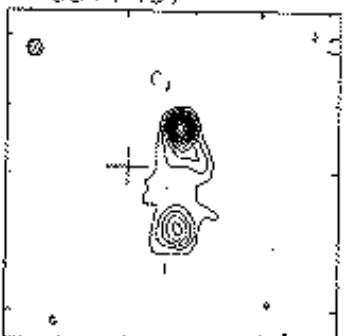


39 25 40

39 25 30

10 29 53 10 29 52

1031+497



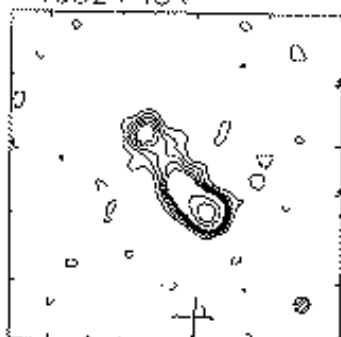
49 48 50

49 48 40

49 48 30

10 31 10 10 31 09

1032+454

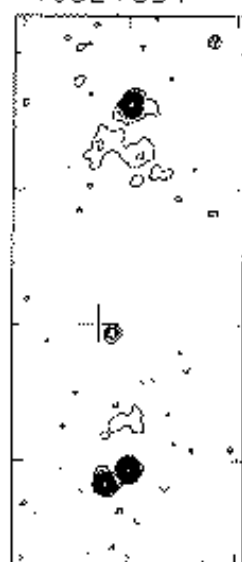


45 26 20

45 26 10

10 32 22 10 32 21 10 32 20

1032+394

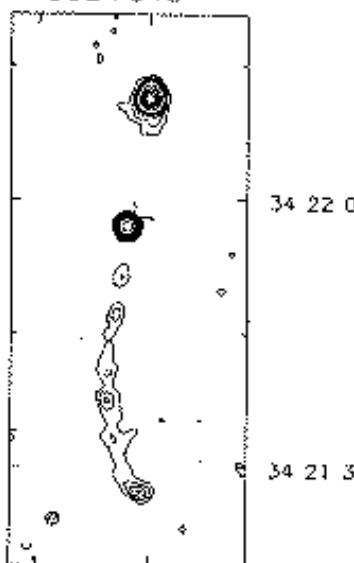


39 26 30

39 26 00

10 32 03 10 32 02 10 32 01

1032+343

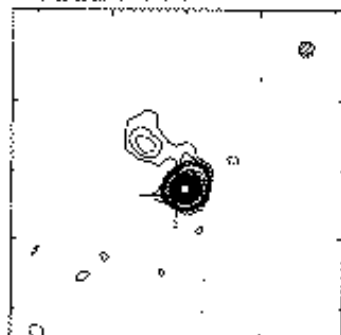


34 22 00

34 21 30

10 32 22 10 32 21

1032+444

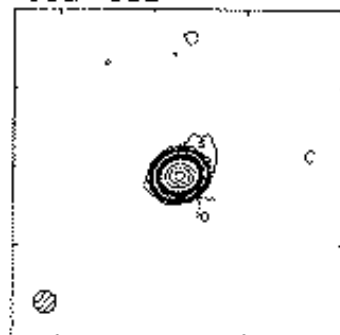


44 25 10

44 25 00

10 32 35 10 32 34

1032+382

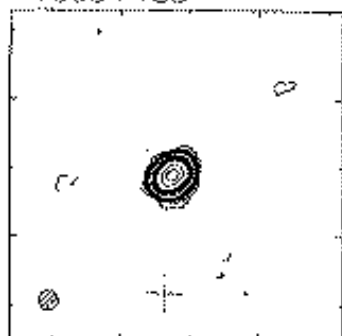


38 12 20

38 12 10

10 32 59 10 32 58

1033+483

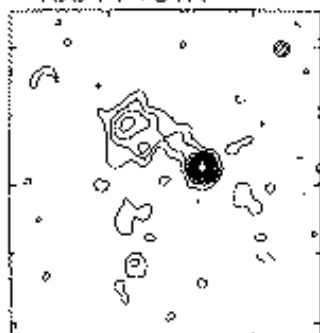


48 22 50

48 22 40

10 33 14 10 33 13

1034+461A



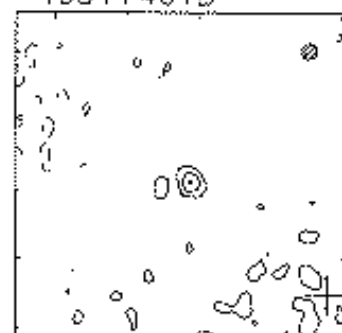
46 09 30

46 08 20

46 09 10

10 34 09 10 34 08

1034+461B

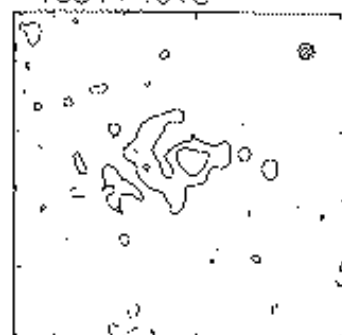


46 07 50

46 07 40

10 34 11 10 34 10 10 34 09

1034+461C

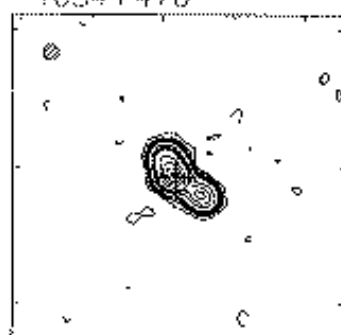


46 10 00

46 09 50

10 34 18 10 34 17 10 34 16

1034+470



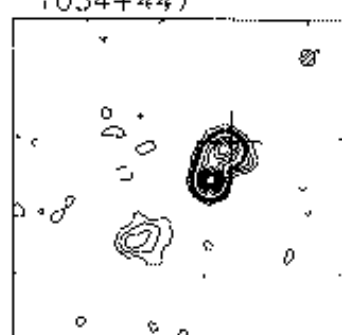
47 05 00

47 05 50

47 05 40

10 34 17 10 34 16 10 34 15

1034+447



44 43 50

44 43 40

10 34 17 10 34 16

1035+389

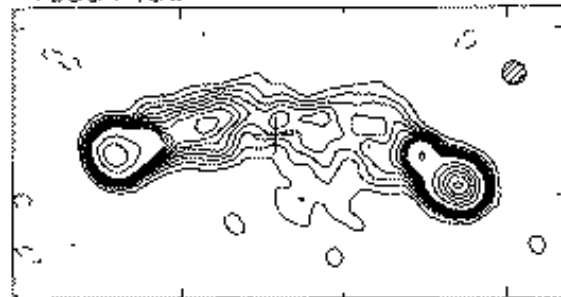


38 56 20

38 56 10

10 35 07 10 35 06

1035+486



48 41 30

48 41 20

10 35 18

10 35 16

1035+500

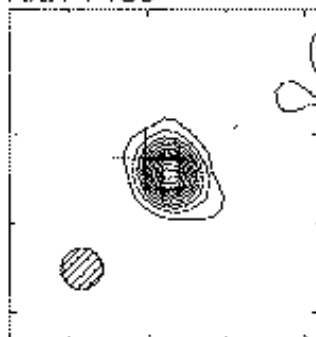


50 03 20

50 03 00

10 35 38 10 35 36

1037+450

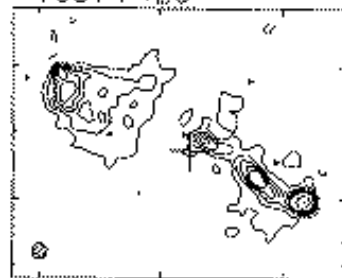


45 05 18

45 05 12

10 37 26 10 37 25.5

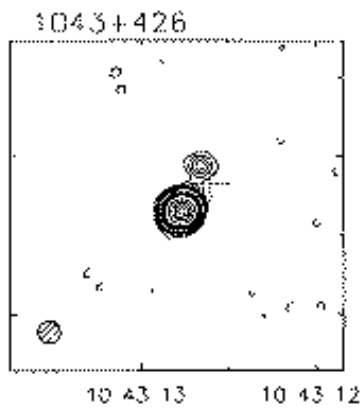
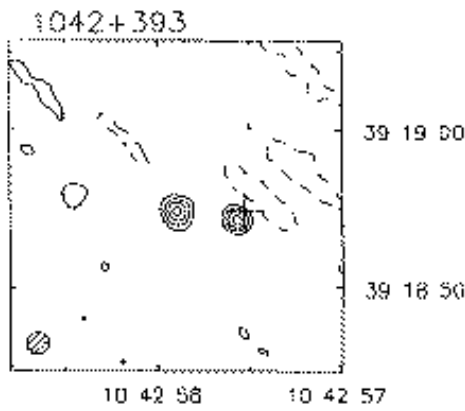
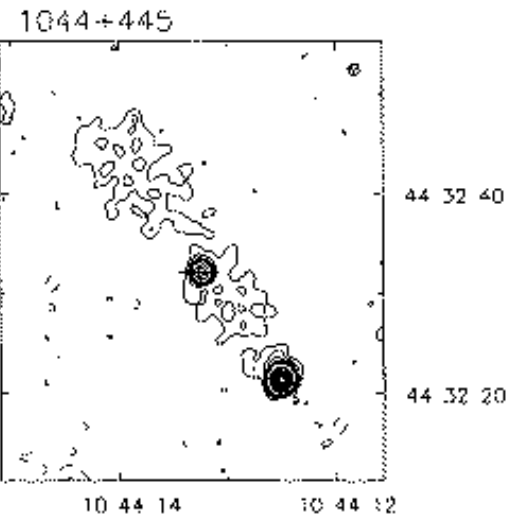
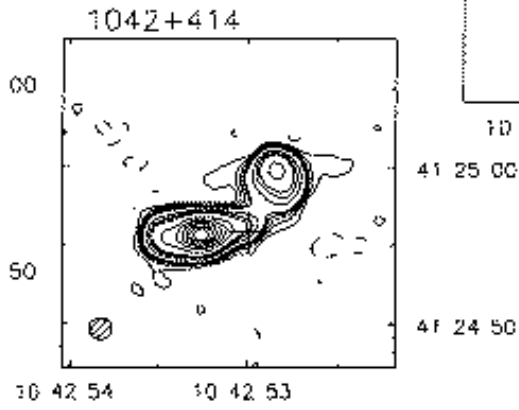
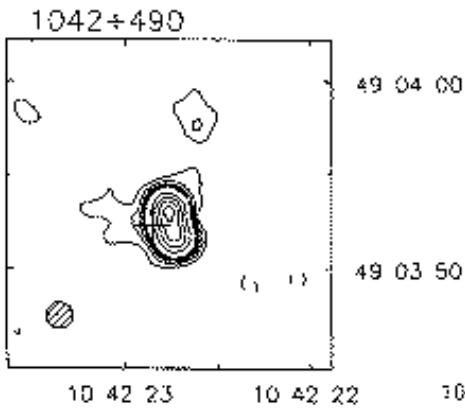
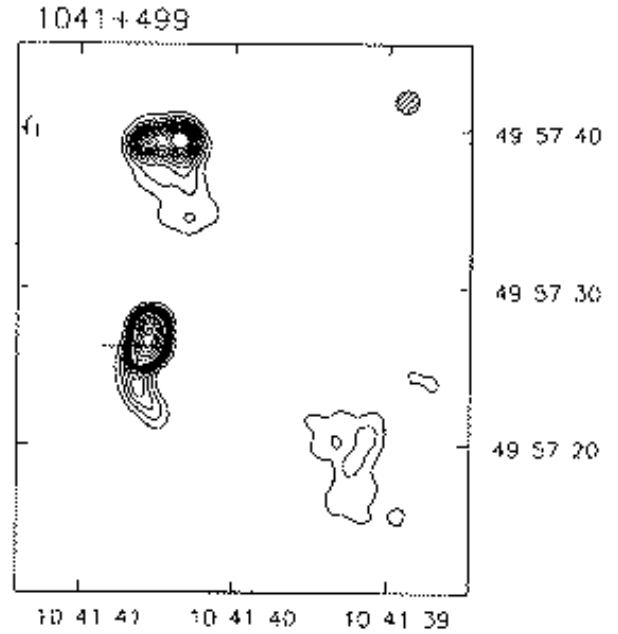
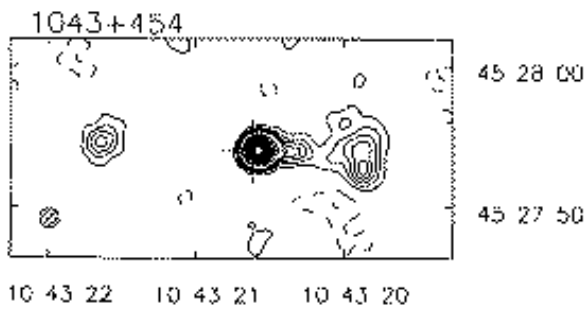
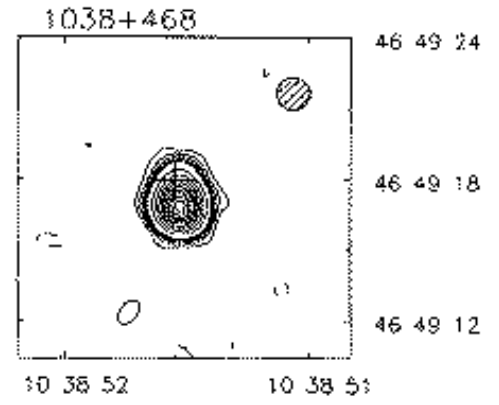
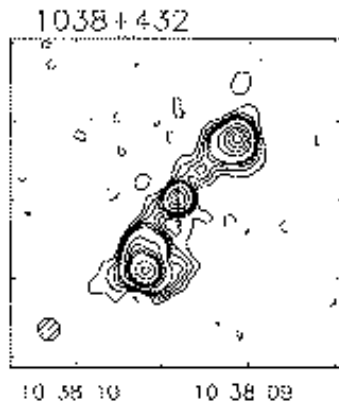
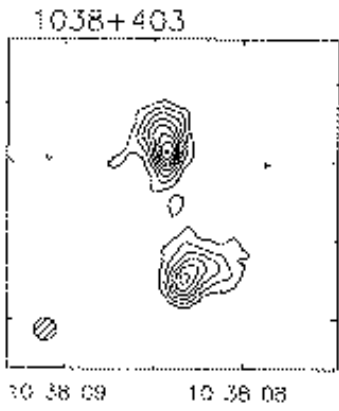
1037+426

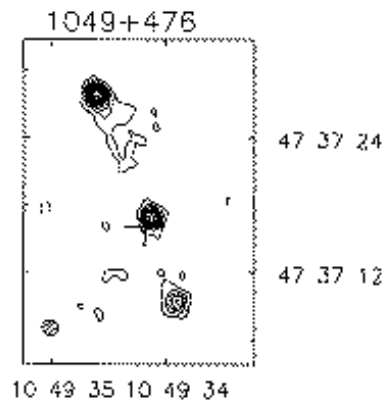
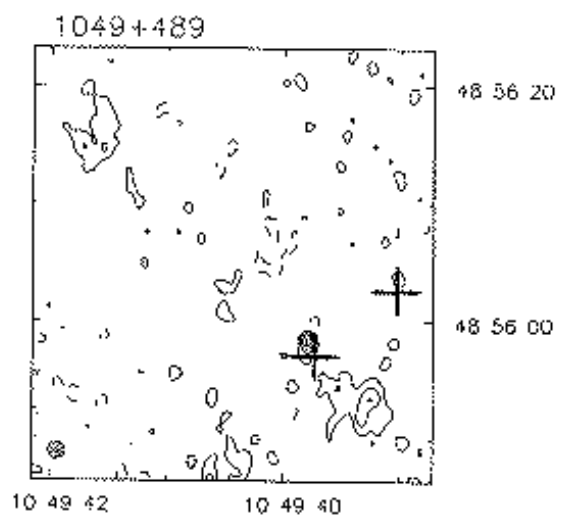
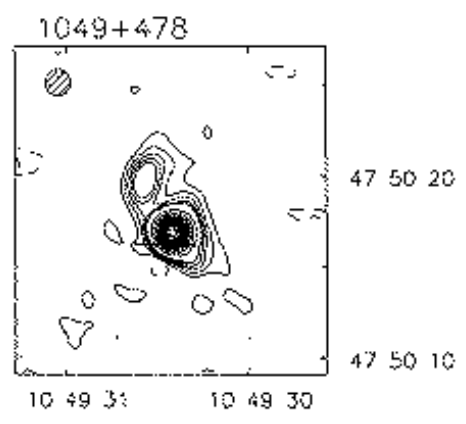
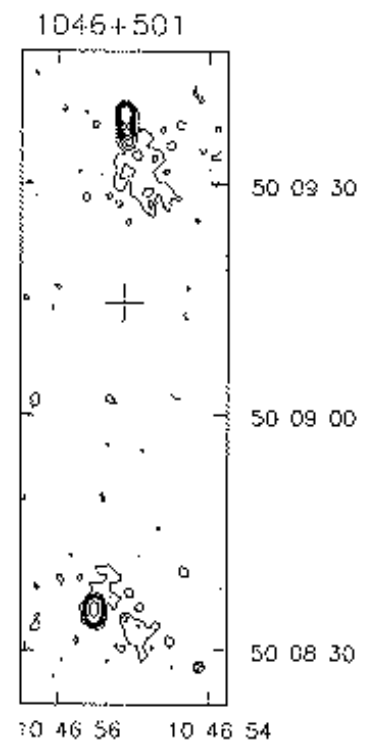
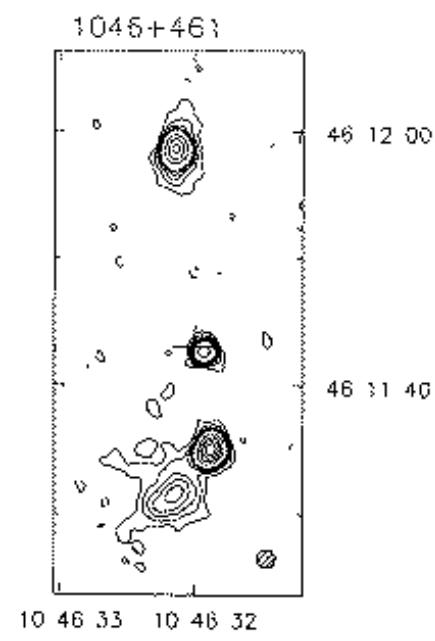
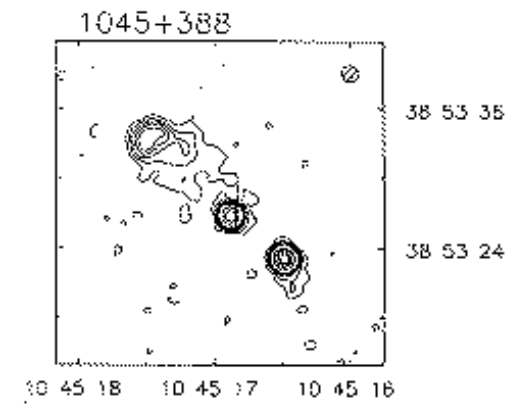
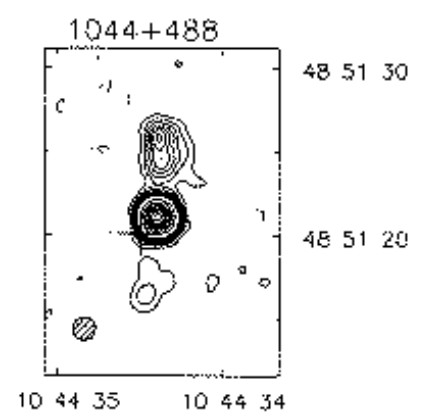
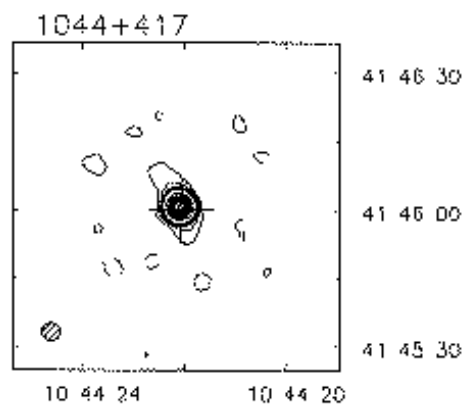
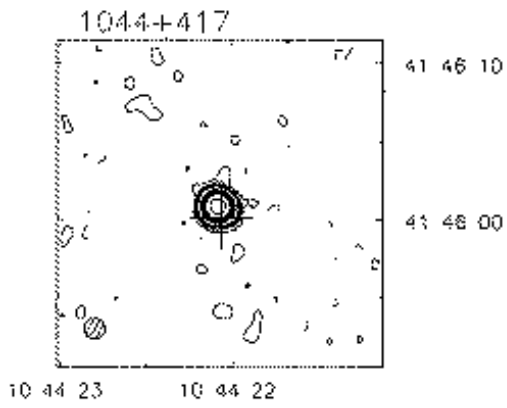


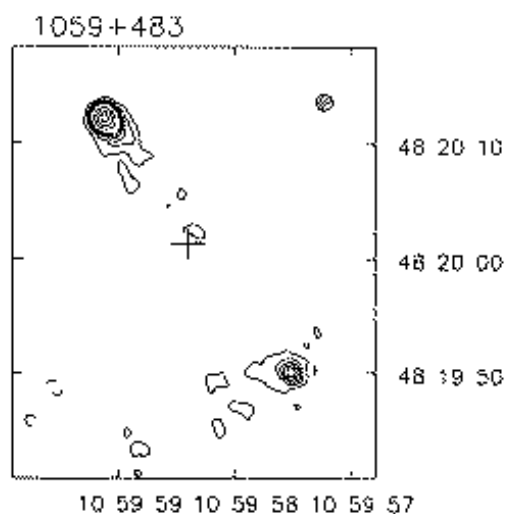
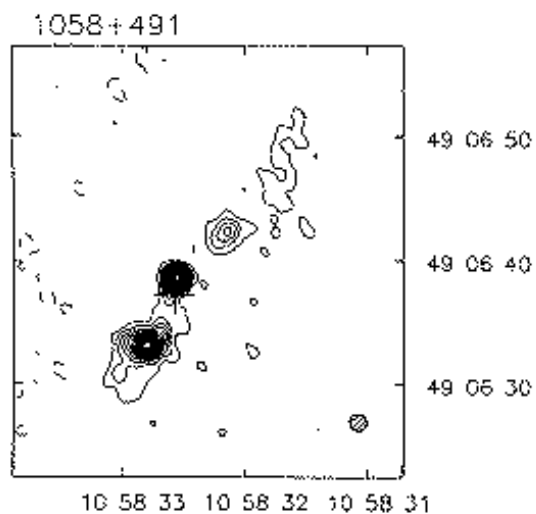
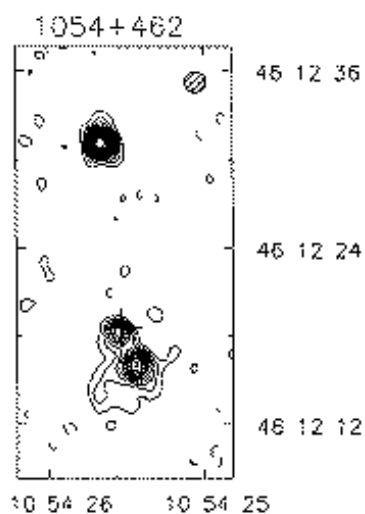
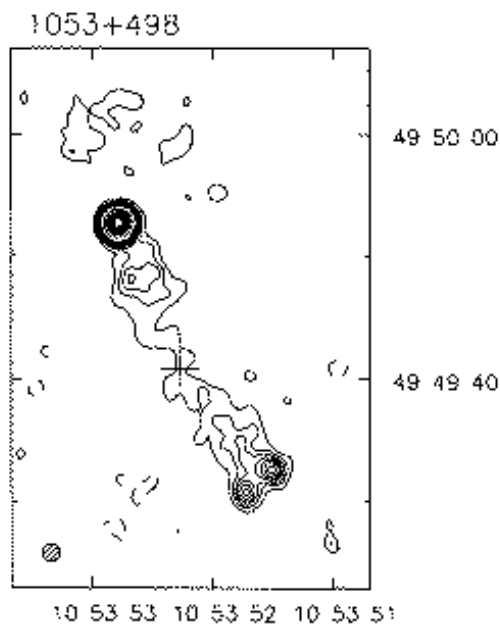
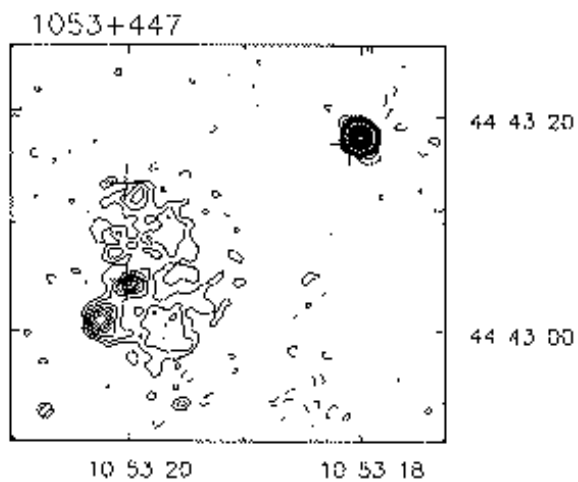
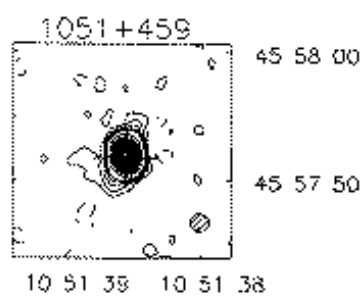
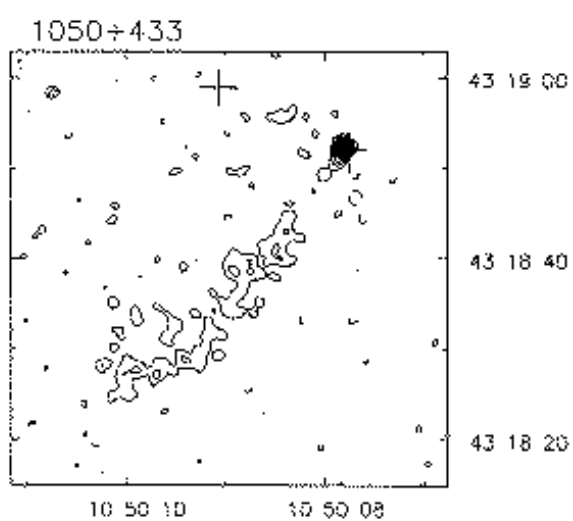
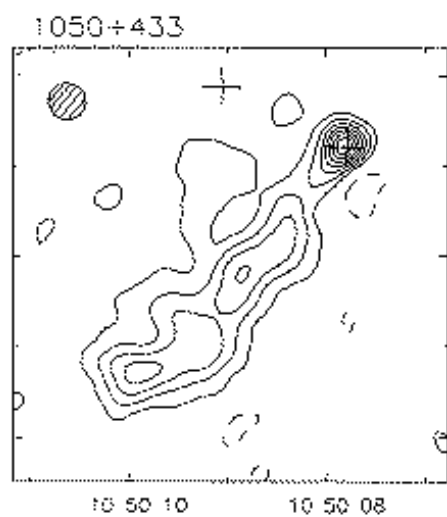
42 41 24

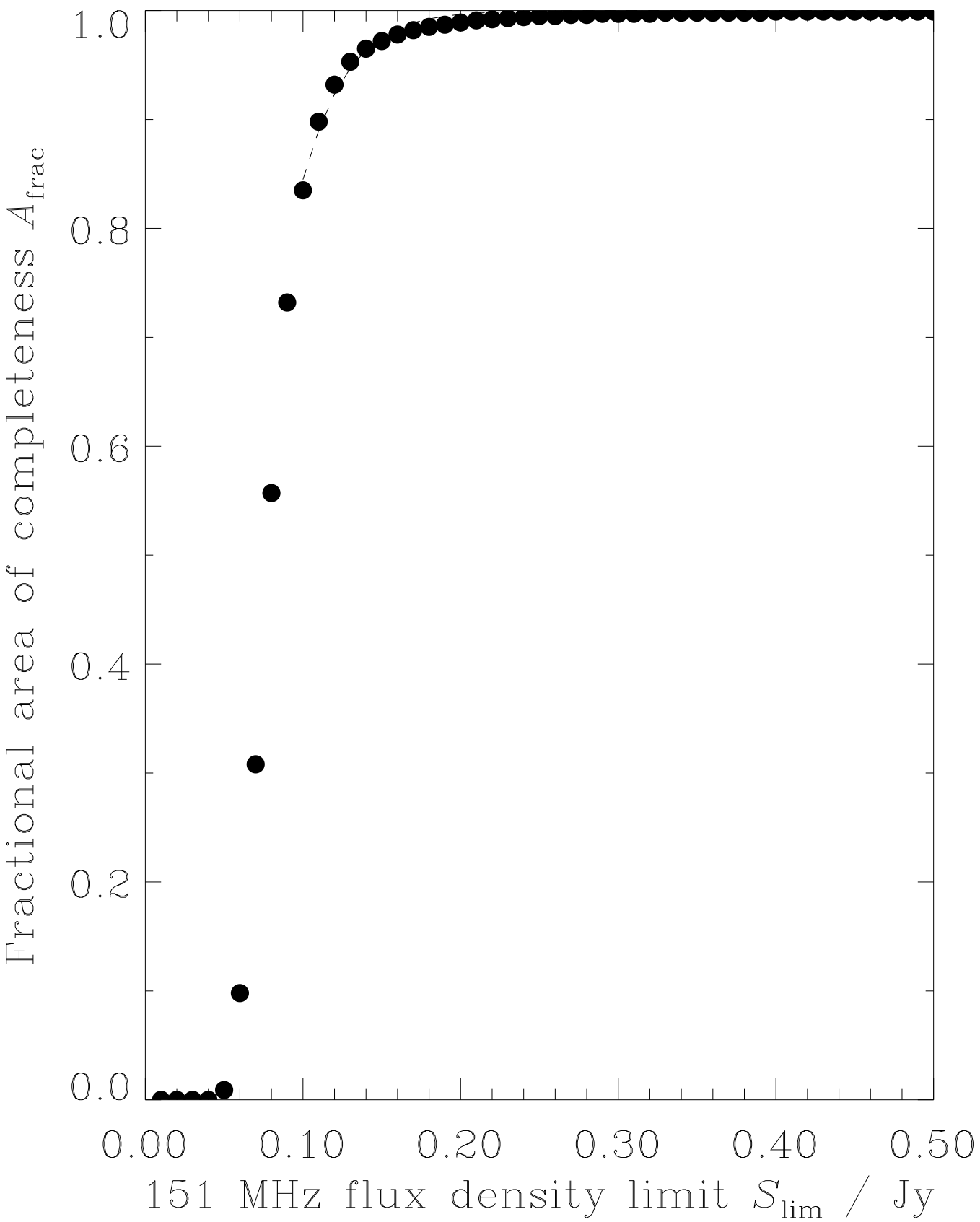
42 41 12

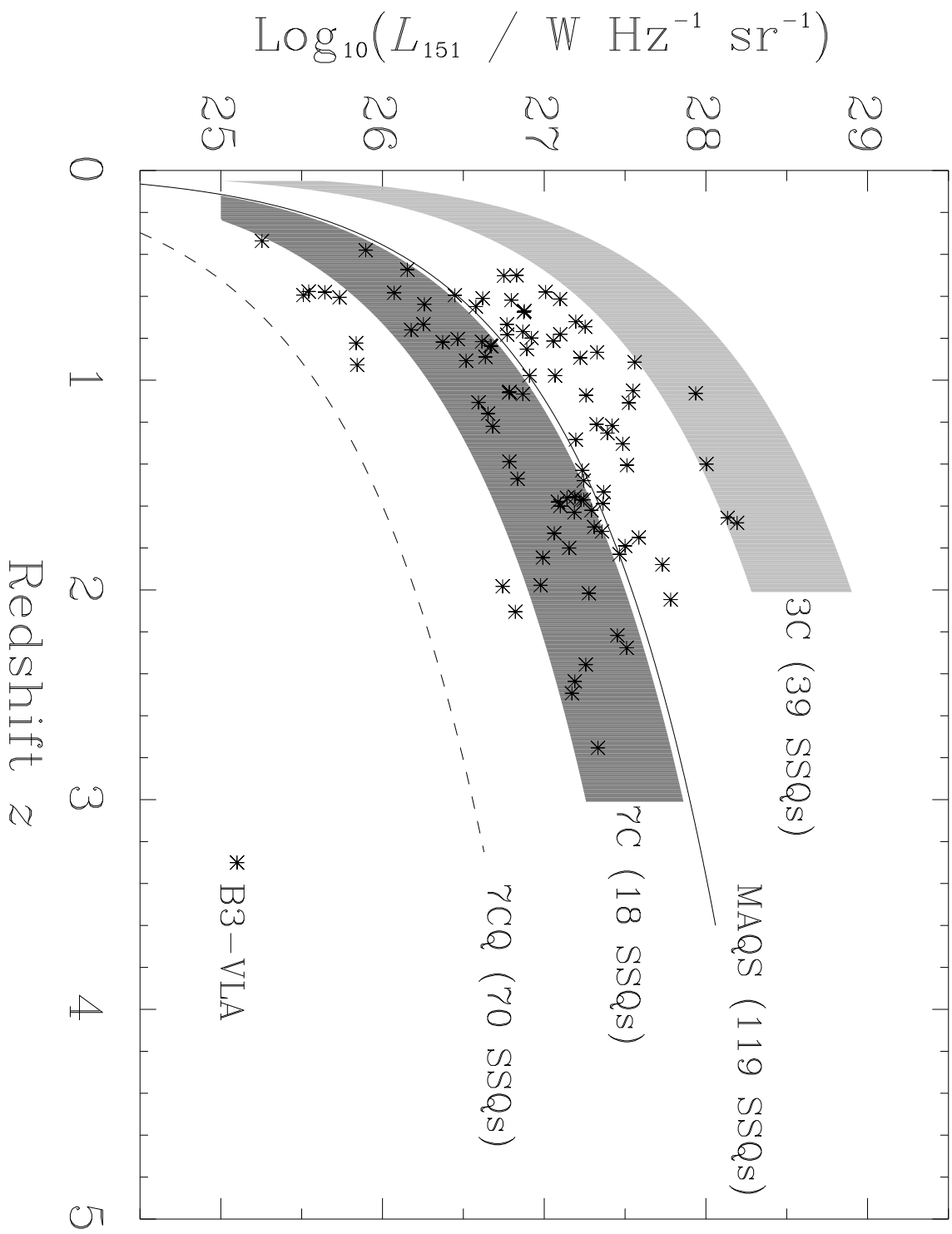
10 37 03 10 37 02 10 37 01



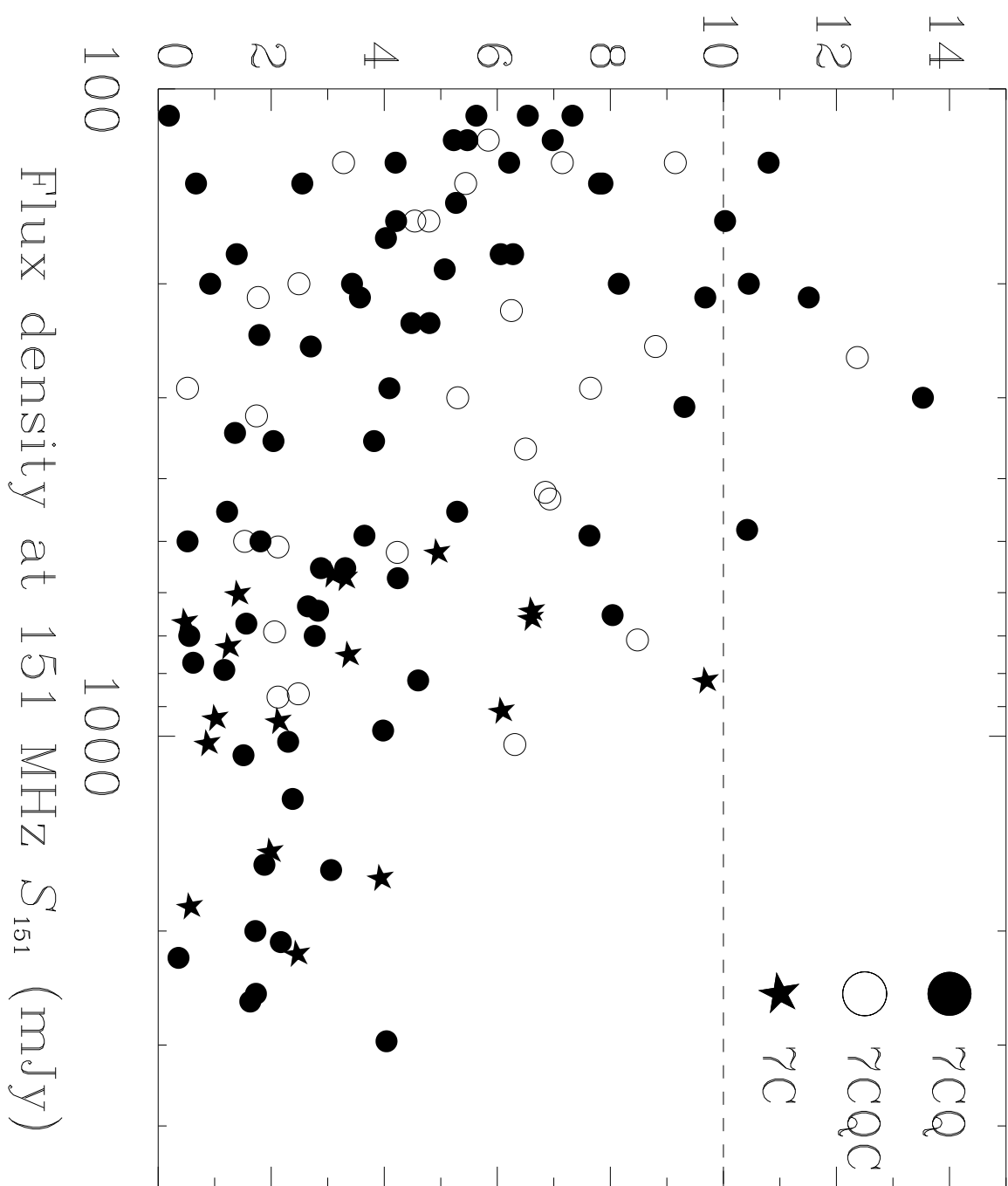








${}^7\text{C}/\text{optical}$ separation r (arcsec)



Declination - B1950.0

